THE COMPUTATION OF PERIODIC SOLUTIONS OF THE 3-BODY PROBLEM USING THE NUMERICAL CONTINUATION SOFTWARE AUTO

D. J. Dichmann*, E. J. Doedel†, R. C. Paffenroth‡

International Conference on Libration Point Orbits and Applications
Aiguablava, Spain, 10-14 June, 2002

Abstract

AUTO2000 is the most recent version of AUTO, a software tool for continuation and bifurcation problems in ordinary differential equations. This paper discusses the continuation methods and bifurcation-detection algorithms that underlie the AUTO2000 software, and describes a method for computing families of periodic solutions of conservative systems. This software package has a number of features that make it useful as a space mission analysis and design tool. Using scripts written in the object-oriented scripting language Python to drive AUTO2000, we have computed several families of periodic solutions emanating from libration points in the Circular Restricted 3-Body Problem (CR3BP) for the Earth-Moon system. By following branches of solutions we were able to locate a variety of periodic orbits that may be useful for space missions. For some of these orbits we gain greater insight by viewing the orbits in both rotating and inertial coordinates. In particular we discuss the family of "Backflip" periodic orbits in which a series of Double Lunar Swingbys can be used to periodically send a spacecraft beyond the ecliptic plane.

1 INTRODUCTION

In space mission design, the availability of a wider range of orbits gives the mission analyst more flexibility in the choice of trajectory, and may lead to new opportunities for observations. In this paper we describe AUTO2000 [13], the most recent version of AUTO, a software tool for continuation and bifurcation problems in ordinary differential equations. We show how AUTO2000 can be used to compute families of periodic solutions of conservative systems, i.e., systems having a first integral. The method is applied to the computation of periodic solutions of the Circular Restricted 3-Body Problem (CR3BP). The CR3BP is a valuable model for space mission design because it has many of the essential features of a more complex high-fidelity force model, yet it is simple enough to lend itself to analysis and computation of families of periodic orbits. A solution of the CR3BP then provides an excellent first approximation of a trajectory in the high-fidelity force model.

The computation at the heart of many mathematical models of physical systems is the solution of a parameter-dependent system of nonlinear equations. Such problems generally have more than one

*Astrodynamics Consultant, Torrance CA
†Department of Computer Science, Concordia University, Montreal
‡Applied and Computational Mathematics, California Institute of Technology

solution, and it is often desirable to compute a family of solutions and search for specific solutions with certainly desirable properties. A bifurcation diagram is a schematic representation of such a solution set. The computation of such bifurcation diagrams and their singularities, e.g., folds, bifurcation points etc., is the domain of numerical continuation algorithms. In Section 2, we review some basic notions of numerical continuation.

The basic idea of the method for continuing a family of periodic orbits in a conservative system was already used in Doedel *et al.* [9]; a more extensive analysis of the ideas in this paper can be found in Doedel *et al.* [14, 44, 48]. The problem of computing a periodic orbit can be phrased as a two-point boundary value problem. However, in a Hamiltonian system such as the CR3BP, the continuation methods implemented in AUTO2000 are not directly applicable, because the existence of a first integral implies non-uniqueness of solutions when the problem is phrased as a two-point boundary value problem in the canonical way. In this paper we describe how such boundary value problems may be modified to account for the Hamiltonian structure. In Section 3, we show how the CR3BP problem may be reformulated using the above ideas so that we may apply numerical continuation methods.

Our focus in this paper is on orbits in the Earth-Moon system. To understand better the physical properties of these orbits, we present in Section 4 the unit conversions to transform from the nondimensional barycentric, rotating system of the CR3BP into physical units for the Earth-Moon system. In Section 5 we use the formulation in Section 3 to compute families of periodic solutions emanating from the L_1 libration point. The numerical continuation methods in AUTO2000 are not restricted to a neighborhood of the libration point, do not depend on any symmetry properties of the solution, and can compute periodic orbits of arbitrary extent until some singularity is reached, such as a collision with a primary. AUTO2000 provides for detection and continuation of bifurcating branches of solutions, so a detailed map of periodic orbits may be computed for each of the libration points for any given value of the ratio of the masses of the primaries. We give graphical results that illustrate the solution structure of periodic orbits emanating from the L_1. All of the branches of solutions shown in Section 5 were generated automatically using a single script written in the object-oriented scripting language Python to drive AUTO2000 [47]. These periodic orbits include the Lyapunov orbits of the planar CR3BP model. However, the three-space dimension model has a much richer periodic solution structure, containing many bifurcations that can be detected easily in our two-point boundary value problem continuation approach. The resulting bifurcation diagram contains some well-known solutions such as the Halo orbits, whose behavior and stability properties have been computed before. (See, for example Howell [35] for a detailed numerical study.) Moreover, the approach used in this paper also generates families of periodic solutions that appear to be less well known, though some appear in articles such as Zagouras and Kazantzis [58].

It is convenient to compute solutions of the CR3BP in rotating coordinates because the equations of motion are autonomous in that frame. However, in Section 6 we show that in some cases one can gain further insight by also visualizing the orbits in Earth Centered Inertial (ECI) coordinates. Finally, in Section 7, we discuss possible applications of some of the families of periodic orbits to space missions, both for scientific and operational space weather observations. We pay particular attention to a family of "Backflip" periodic orbits, reminiscent of the Backflip maneuver described by Uphoff [56], in which a periodic Double Lunar Swingby allows a spacecraft to explore the space both near and beyond the ecliptic plane.

The AUTO2000 source code is publicly available via HTTP from the web site:

http://auto2000.sourceforge.net.

2 CONTINUATION OF SOLUTIONS

Most existing numerical continuation algorithms are for the computation of one-dimensional solution manifolds called *solution branches*, e.g., H. B. Keller [41], Allgower and Georg [1], Doedel et al. [11, 12] and Rheinboldt [49]. To review the basic notions of continuation, first consider the finite-dimensional equation

$$\mathbf{F}(\mathbf{y}, \lambda) = \mathbf{0}, \qquad \mathbf{F} \; : \; \mathbb{R}^n \times \mathbb{R} \; \rightarrow \; \mathbb{R}^n, \tag{1}$$

where the bold font indicates a vector, $\mathbf{F}$ is assumed to be sufficiently smooth for the theory to apply, $\mathbf{y} \in \mathbb{R}^n$, and $\lambda \in \mathbb{R}$. One may also write Equation 1 as $\mathbf{F}(\mathbf{x}) = \mathbf{0}$ by setting $\mathbf{x} = (\mathbf{y}, \lambda)$, and we will use this notation when the distinction between the components $\mathbf{y}$ and λ is not pertinent. This system has one more variable than it has equations. Given a solution $(\mathbf{y}_0, \lambda_0)$, there generally exists a locally unique one-dimensional family of points, called a solution branch, that passes through $(\mathbf{y}_0, \lambda_0)$. To compute another nearby point $(\mathbf{y}_1, \lambda_1)$ on this branch, one can use a root-finding procedure, such as Newton's method, to solve the extended system

$$\begin{array}{ll} \text{a)} & \mathbf{F}(\mathbf{y}, \lambda) = \mathbf{0}, \\ \text{b)} & \lambda = \lambda_0 + \Delta\lambda, \end{array} \tag{2}$$

using as an initial guess $(\mathbf{y}_0, \lambda_1)$. In general $\mathbf{F}(\mathbf{y}_0, \lambda_1) \neq \mathbf{0}$, but if the step size $\Delta\lambda$ is sufficiently small, and $\mathbf{F}$ is sufficiently smooth, then $(\mathbf{y}_0, \lambda_1)$ lies within the basin of attraction of the given root-finding procedure, so the procedure converges to $(\mathbf{y}_1, \lambda_1)$. Note, in this case, the initial guess $(\mathbf{y}_0, \lambda_1)$ already satisfies Equation 2b, so in practice only Equation 2a need be solved for $\mathbf{y}$. This algorithm is called *natural parameter continuation* and is shown schematically in Figure 1.

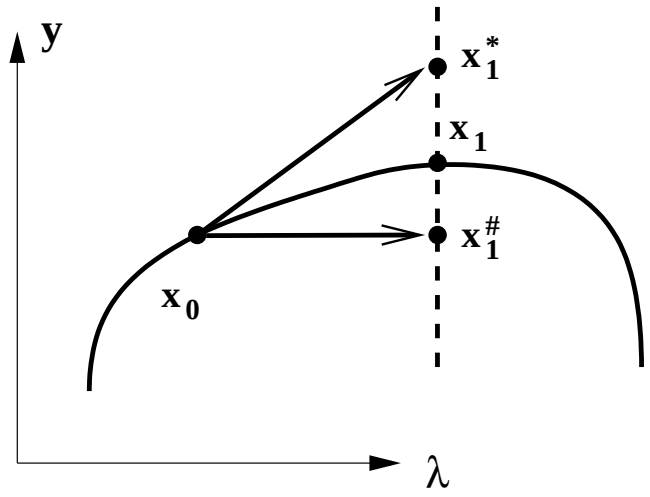

Figure 1: Natural parameter continuation with two different initial approximations: Solving Equation 2 using Newton's method entails the selection of an initial approximation. For example, one can use the approximation $\mathbf{x}_1^\# = (\mathbf{y}_0, \lambda_1)$. On the other hand, one might want to use a higher-order approximation. For example, given $\dot{\mathbf{x}}_0$, the unit tangent to the solution curve at $\mathbf{x}_0$, one can use $\mathbf{x}_1^* = \mathbf{x}_0 + \dot{\mathbf{x}}_0 \, \Delta s$ as a more accurate initial approximation, where Δs is chosen to have $\mathbf{x}_1$ lie on the line $\lambda = \lambda_1$.

One may now iterate the procedure described in the previous paragraph: $\mathbf{x}_0 = (\mathbf{y}_0, \lambda_0)$ is used to compute $\mathbf{x}_1 = (\mathbf{y}_1, \lambda_1)$, which in turn in used to compute $\mathbf{x}_2$, etc. As shown in Figure 2, the core principle of numerical continuation is that, under certain conditions on $\mathbf{F}$, the solution branch is surrounded by a basin of attraction for Newton's method. If we have a starting value $\mathbf{x}_0$ on the solution branch then, if the step size is sufficiently small, all steps stay within the basin of attraction and Newton's method converges for all steps of the calculation. On the other hand, if one were to

search directly for a solution where $\lambda = \lambda_{desired}$, and one did not have a good initial approximation, then there is no guarantee Newton's method would converge.

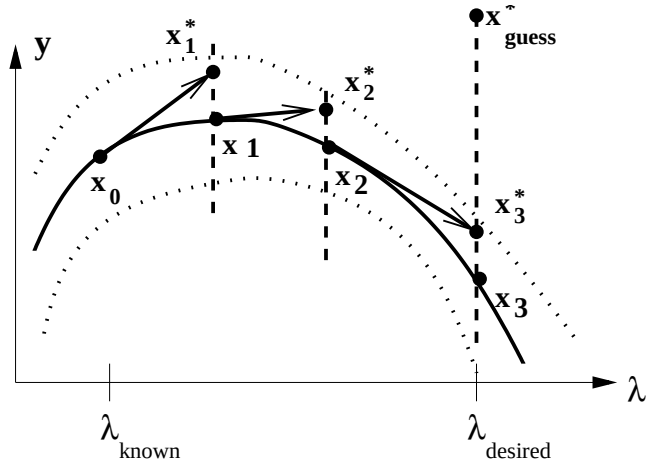

Figure 2: Staying within the basin of attraction: The core principle of numerical continuation is that, under certain conditions on $\mathbf{F}$, the solution branch is surrounded by a basin of attraction for Newton's method. Here the basin of attraction is shown as the region bounded by dotted lines. If we have a starting value $\mathbf{x}_0 = (\mathbf{y}_0, \lambda_0)$ on the solution branch, then step sizes can be chosen so that all steps stay within the basin of attraction and Newton's method converges. On the other hand, if one were to directly search for a solution where $\lambda = \lambda_{desired}$, and did not have a good initial approximation such as $\mathbf{x}^*_{guess}$, then there is no guarantee Newton's method would converge.

Natural parameter continuation captures the central ideas of numerical continuation, but it has some weaknesses. One significant problem with natural parameter continuation is that it fails at a *fold*, such as the one shown in Figure 3, because it does not account for the local shape of the solution curve. To formulate a method which can compute around folds, we begin by constructing an initial approximation to $\mathbf{x}_1$ as $\mathbf{x}^*_1 = \mathbf{x}_0 + \dot{\mathbf{x}}_0 \, \Delta s$, for some step size Δs, where $\dot{\mathbf{x}}_0$ is the unit tangent to the solution curve at $\mathbf{x}_0$. If we differentiate Equation (1) with respect to the arclength s at $\mathbf{x}_0$, we find $\mathbf{F}_\mathbf{x}(\mathbf{x}_0)\, \dot{\mathbf{x}}_0 = 0$. Thus the vector $\dot{\mathbf{x}}_0$ is a null vector of the Jacobian matrix $\mathbf{F}_\mathbf{x}(\mathbf{x}_0)$, and can be computed at little cost. However the higher-order approximation does not, by itself, suffice to compute around a fold because there may be no solutions for the desired value of λ. One must allow values of λ to be determined by the geometry of the solution curve. Accordingly, we replace the system in Equation 2 with

$$\begin{array}{ll} \text{a)} & \mathbf{F}(\mathbf{x}_1) = \mathbf{0}, \\ \text{b)} & (\mathbf{x}_1 - \mathbf{x}_0)^T \dot{\mathbf{x}}_0 = \Delta s, \end{array} \tag{3}$$

where the superscript T denotes the transpose. The magnitude of the step size Δs is normally adapted along the branch, depending for example on the convergence rate of Newton's method. The result is a well-known algorithm, called the *pseudo-arclength continuation method* [41], and is shown schematically in Figure 3. The name pseudo-arclength arises from the fact that the step size Δs approximates the arclength along the curve.

It can be shown that the above continuation method works if $\mathbf{x}_0$ is a *regular solution*, i.e., if the null space of $\mathbf{F}_\mathbf{x}(\mathbf{x}_0)$ is one-dimensional. In this case the Jacobian of Equation 3 evaluated at $\mathbf{x}_0$, i.e., the $n+1$ by $n+1$ matrix

$$\begin{pmatrix} \mathbf{F}_\mathbf{x}(\mathbf{x}_0) \\ \dot{\mathbf{x}}_0^T \end{pmatrix}, \tag{4}$$

can easily be shown to be nonsingular. By the Implicit Function Theorem, this guarantees the existence of a locally unique solution branch through $\mathbf{x}_0$. This branch can be parameterized locally

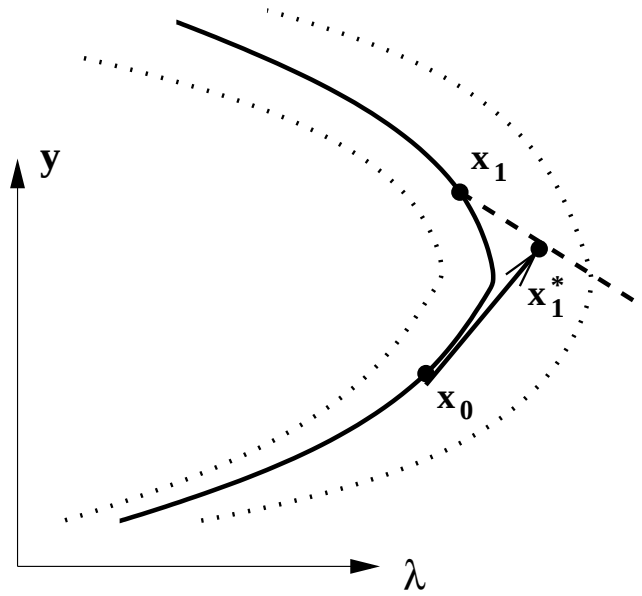

Figure 3: Pseudo-arclength continuation and folds: Instead of fixing the value of λ, we add a constraint as shown in Equation 3b which implies the new solution $\mathbf{x}_1$ we compute lies in the hyperplane perpendicular to the tangent vector $\dot{\mathbf{x}}_0$. In this way, the value of λ is allowed to vary, and is computed as one of the solution components using Newton's method. As this figure indicates, pseudo-arclength continuation is well-suited for numerical continuation around folds.

by Δs. Moreover, for Δs sufficiently small and the initial approximation $\mathbf{x}_1^{(0)} = \mathbf{x}_0 + \dot{\mathbf{x}}_0 \Delta s$, Newton's method for solving (3) can be shown to converge.

In this paper we focus on the problem of computing a branch of periodic solutions of a dynamical system

$$\mathbf{x}'(t) = \mathbf{f}\big(\mathbf{x}(t), \lambda\big), \qquad \mathbf{f} \;:\; \mathbb{R}^n \times \mathbb{R} \;\rightarrow\; \mathbb{R}^n, \tag{5}$$

where $\lambda \in \mathbb{R}$ is a physical parameter. In this case the continuation step corresponding to Equation 3 takes the form of the constrained periodic boundary value problem

$$\begin{array}{ll} \mathrm{a}_1) & \mathbf{x}_1'(\tau) = T_1 \mathbf{f}\big(\mathbf{x}_1(\tau), \lambda_1\big), \\ \mathrm{a}_2) & \mathbf{x}_1(0) = \mathbf{x}_1(1), \\ \mathrm{a}_3) & \int_0^1 \mathbf{x}_1(\tau)^T \; \dot{\mathbf{x}_0}(\tau) \; d\tau = 0, \\ \mathrm{b}) & \int_0^1 \big(\mathbf{x}_1(\tau) - \mathbf{x}_0(\tau)\big)^T \dot{\mathbf{x}}_0(\tau) \; d\tau + (T_1 - T_0)\dot{T}_0 + (\lambda_1 - \lambda_0)\dot{\lambda}_0 = \Delta s. \end{array} \tag{6}$$

These equations are to be solved for $(\mathbf{x}_1(\cdot), T_1, \lambda_1)$, given a solution $(\mathbf{x}_0(\cdot), T_0, \lambda_0)$ and the tangent $(\dot{\mathbf{x}}_0(\cdot), \dot{T}_0, \dot{\lambda}_0)$. Here $T_1 \in \mathbb{R}$ is the unknown period, and τ is a scaled independent variable such that the periodic solution has period 1 as a function of τ. Equation 6a$_2$ imposes unit periodicity. Equation 6a$_3$ is a phase condition, which fixes the phase of the new orbit $\mathbf{x}_1(\cdot)$ relative to the given orbit $\mathbf{x}_0(\cdot)$. This integral phase condition has the desirable property of minimizing phase drift relative to $\mathbf{x}_0(\cdot)$. Equation 6b is the functional form of the pseudo-arclength constraint 3b. For full details on this formulation see Doedel *et al.* [12].

Equation 6 can be solved by numerical boundary value solvers. In particular, AUTO [10] uses piecewise polynomial collocation, similar to COLSYS [2], with adaptive mesh selection as described in Russell and Christiansen [53]. By using collocation, Equation 6 becomes a discrete system of the form of Equation 1, which can be solved using the continuation methods described in this section. For full details see [12].

3 PERIODIC SOLUTIONS OF THE CIRCULAR RESTRICTED 3-BODY PROBLEM

Section 2 described the mathematical formulation of problems that may be addressed by numerical continuation methods. In this section we show how the Circular Restricted 3-Body Problem (CR3BP) can be expressed in the form of Equation 5.

The CR3BP describes the dynamics of a body with negligible mass under the gravitational influence of two massive bodies, called the primaries, where the primaries move in circular orbits about their barycenter. Let (x, y, z) denote the position of the negligible-mass body in a rotating coordinate system with the origin at the barycenter where the x-axis points from the larger to the smaller primary; the z-axis points along the vector normal to the orbit plane of the primaries; and the y-axis completes the right-handed orthogonal triad. The parameter μ represents the ratio of the mass of the smaller primary to the total mass. In this paper we consider the Earth-Moon system, for which $\mu = 0.01215$. The units are chosen so that the distance between the primaries, the sum of the masses of the primaries and the angular velocity of the primaries are all equal to one. Consequently the larger and smaller primaries are located at $(-\mu, 0, 0)$ and $(1-\mu, 0, 0)$, respectively. The equations of motion for the CR3BP are

$$\begin{aligned} x'' &= 2y' + x - (1-\mu)(x+\mu)r_1^{-3} - \mu(x-1+\mu)r_2^{-3}, \\ y'' &= -2x' + y - (1-\mu)yr_1^{-3} - \mu yr_2^{-3}, \\ z'' &= -(1-\mu)zr_1^{-3} - \mu zr_2^{-3}, \end{aligned} \tag{7}$$

where

$$r_1 = \sqrt{(x+\mu)^2 + y^2 + z^2}, \qquad r_2 = \sqrt{(x-1+\mu)^2 + y^2 + z^2}.$$

A derivation of these equations can be found in Danby [6].

The dynamical system in Equation 7 has one integral of motion, namely the Jacobi integral

$$C = 2\ U(x, y, z) - (v_x^2 + v_y^2 + v_z^2),$$

where $v_x = x'$, $v_y = y'$, $v_z = z'$ and

$$U(x, y, z) = \frac{1}{2}(x^2 + y^2) + \frac{1-\mu}{r_1} + \frac{\mu}{r_2}.$$

It is well-known that for each value of μ this system has five equilibria, called libration points (or Lagrange points) [54], which lie in the orbit plane of the primaries. Three of the libration points, denoted L_1, L_2 and L_3, are collinear with the primary bodies; one of them, L_1, lies between the two primaries. Each of the other two points, L_4 and L_5, forms an equilateral triangle with the primaries. There exist two well-known families of periodic solutions near each of the collinear libration points: the Lyapunov orbits that lie in the $x-y$ plane, and the so-called Vertical orbits that arise from the purely vertical solutions in the linearized dynamics [36]. In this paper we use numerical continuation methods to explore families of three-dimensional periodic solutions of Equation 7 that emanate from L_1.

We make three modifications to Equation 7 to obtain a system to which AUTO2000 and numerical continuation may be applied. First, the three-dimensional second-order system in Equation 7 is rewritten as a six-dimensional first-order system in the standard way because AUTO2000 is set up to handle first-order systems. Second, we perform the transformation in Equation 6 where we add boundary conditions which impose unit periodicity, a phase constraint, and we introduce the unknown period T which we solve for as part of the numerical continuation procedure.

The final modification is introduced to allow us to use the continuation method described in Section 2 to compute periodic solutions of the CR3BP. The Circular Restricted 3-Body Problem is a

conservative system, for which there exists a first integral. Such systems have special structure, and a theorem that one can apply in such a context is the Cylinder Theorem [43]: An elementary periodic orbit of a system with an integral I lies in a smooth cylinder of periodic solutions parameterized by I. The Cylinder Theorem implies there exists a branch of periodic orbits in a system without a parameter. However the theory and algorithms developed in Section 2, and especially Equations 5 and 6, rely on the presence of a parameter. To take advantage of the power of numerical continuation methods we must rephrase the problem in a form where such methods can be applied directly. We accomplish this with the introduction of an "unfolding parameter" λ, which is treated as an unknown but which will be zero upon solution. For a further background on this technique, see [14, 44, 48].

The resulting system of differential equations is

$$\begin{aligned}
x' &= Tv_x + \lambda\ \partial C/\partial x, \\
y' &= Tv_y + \lambda\ \partial C/\partial y, \\
z' &= Tv_z + \lambda\ \partial C/\partial z, \\
v_x' &= T[2v_y + x - (1-\mu)(x+\mu)r_1^{-3} - \mu(x-1+\mu)r_2^{-3} + \lambda\ \partial C/\partial v_x], \\
v_y' &= T[-2v_x + y - (1-\mu)yr_1^{-3} - \mu yr_2^{-3} + \lambda\ \partial C/\partial v_y], \\
v_z' &= T[-(1-\mu)zr_1^{-3} - \mu zr_2^{-3} + \lambda\ \partial C/\partial v_z],
\end{aligned} \tag{8}$$

with separated boundary conditions

$$\begin{aligned}
&x(1) = x(0), \quad && y(1) = y(0), \quad && z(1) = z(0), \\
&v_x(1) = v_x(0), \quad && v_y(1) = v_y(0), \quad && v_z(1) = v_z(0),
\end{aligned} \tag{9}$$

where T is the unknown period, and λ is the unfolding parameter.

4 PHYSICAL UNITS

In order to relate the nondimensional units discussed in this paper to the physical world we need to be able to describe them in engineering units. We will use the superscript * to denote quantities in physical units.

The gravitational constants of the Earth and the Moon are $GM^*_{Earth} = 398600.5$ km^3/sec^2 and $GM^*_{Moon} = 4902.794$ km^3/sec^2, so that $\mu = 0.01215$. Let $GM^* = GM^*_{Earth} + GM^*_{Moon} = 403503.3$ km^3/sec^2. We take the Earth-Moon distance to be $R^* = 384401$ km, the Earth's radius to be 6378 km $= 0.0165\ R^*$, and the Moon's radius to be 1738 km $= 0.0045\ R^*$ [57].

Using Kepler's Third Law the rotational period of the system would be $P^*_{EM} = 2\pi\sqrt{(R^*)^3/GM^*} = 27.2846$ days. In fact, due to third-body effects, the period of the Earth-Moon system is $P^*_{EM} = 27.3217$ days [57]. Because the angular velocity ω_{EM} is set to 1 in the nondimensional rotating coordinate system, the orbit period P_{EM} is 2π in the nondimensional system.

To transform a distance r from nondimensional to physical units we use $r^* = R^* r$. To transform a time t from nondimensional to physical units we use $t^* = P^*_{EM}/P_{EM}\ t = T^*\ t$, where $T^* = P^*_{EM}/(2\pi) = 4.3225$ days. The Jacobi integral C has units of velocity squared, so to transform the Jacobi integral from nondimensional to physical units we use $C^* = (R^*/T^*)^2 C$ where $(R^*/T^*)^2 = 1.049694$ km^2/sec^2. (If P^*_{EM} were derived from Kepler's Law, then we would have $(R^*/T^*)^2 = GM^*/R^*$.)

The period of rotation for the Sun-Earth system in the inertial frame is $P^*_{SE} = 365.256$ days. In terms of the nondimensional Earth-Moon orbit period, the Sun-Earth rotational period is $P_{SE} = P^*_{SE}/T^* = (P^*_{SE}/P^*_{EM})P_{EM} = 13.3687\ P_{EM}$.

5 TOUR OF THE BIFURCATION DIAGRAM

In this section we present a tour of the families of periodic orbits emanating from L_1 that we have computed using AUTO2000. Previous work has mapped portions of the families of periodic orbits for various values of μ; cf. Howell [36] and references therein. Some researchers has investigated bifurcations of these families, including Ichtiaroglou and Michalodimitrakis [39], Hénon [34] and Howell and Campbell [38]. Gómez and Mondelo [32] computed the families of orbits arising from L_1, L_2 and L_3, as well as their bifurcating branches, for the Earth-Moon system

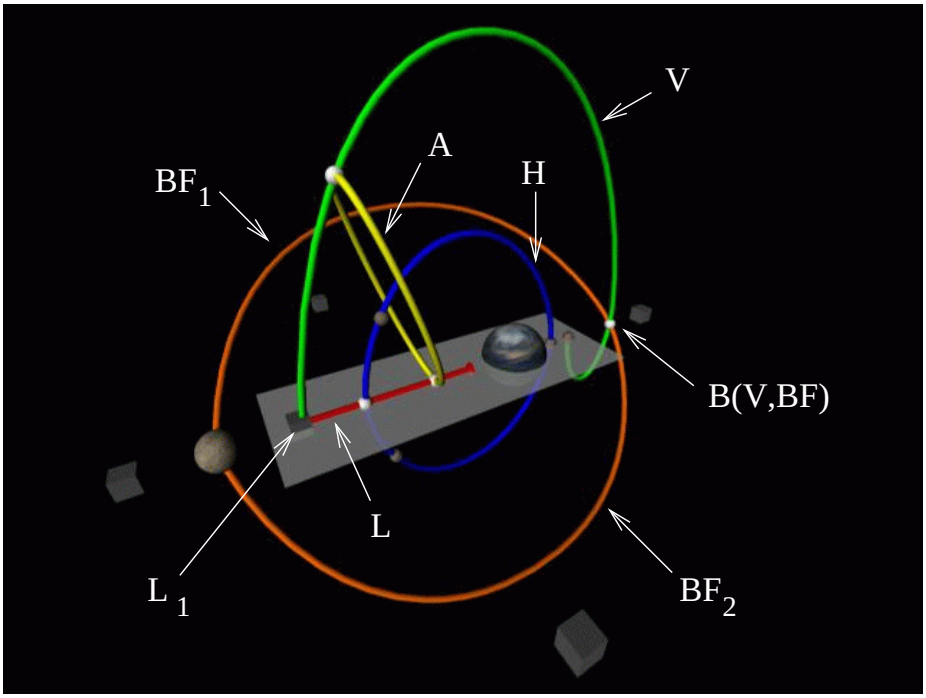

Figure 4: The bifurcation diagram for periodic orbits emanating from L_1: The curves represent some of the branches of periodic solutions computed using AUTO2000. The Earth and Moon are shown as two textured spheres, and the five libration points are shown as cubes. The branch labelled "L" represents the Lyapunov orbits (see Figure 6) and the branch labelled "V" represents the Vertical orbits (see Figure 9). Each bifurcation point is marked as a small white sphere if we discuss the bifurcating branch in this paper; otherwise the bifurcation point is colored brown. The rectangle lies in the $x-y$ plane, and has the property that any solution branch which touches it has a planar solution at that point. For example, the entire branch of Lyapunov orbits lies in the plane, so all the orbits on that branch are planar. Planar orbits are trivially symmetric about the $x-y$ plane. If a solution is symmetric about the $x-y$ plane but nonplanar, then we have depicted it lying in the same plane as the gray rectangle but not touching the gray rectangle. On the branch of Lyapunov orbits there are two bifurcations, the first giving rise to the branch of Halo orbits, labelled by "H" (see Figure 7), and the second giving rise to a branch of "Axial" orbits that connect the Lyapunov and Vertical branches, labelled by "A"(see Figure 8). On the branch of Vertical orbits away from L_1 there are three bifurcations. The second bifurcation point, labelled $B(V, BF)$, yields the orange branches, labelled "BF_1" and "BF_2", that respectively represent the Class 1 and Class 2 families of Backflip orbits (see Figures 10 and 11).

AUTO2000 is designed to follow a branch of solutions, starting from a known or approximate solution, and to locate bifurcation points along the branch. Previous versions of AUTO had a good interface for expert users, but this interface was somewhat difficult for beginners. Accordingly, the detection of families of periodic solutions near a libration point, and the continuation of these

branches was facilitated by a Python script [47]. Near a collinear libration point there are two such branches, the Lyapunov branch and the Vertical branch. The Python script also computes branches that arise from each of the bifurcation points[1] along the branches emanating from the libration point.

Our presentation is organized around the bifurcation diagram shown in Figure 4, in which each curve represents a branch of periodic solutions. Figure 4 and later figures in this section show the Earth and Moon as two textured spheres. The libration points are visualized as cubes, and the branches of periodic orbits are drawn as curves. For example, the branch of Lyapunov orbits, marked with an "L" and the branch of vertical orbits, marked with a "V", both emanate from the cube representing L_1. Each bifurcation point is marked as small white sphere if we follow the bifurcating branch in this paper; otherwise the bifurcation point is colored brown. There are many branches of solutions for this problem, and in this paper we only treat a small subset. In addition, we include a gray rectangle that lies in the $x-y$ plane. Any solution branch that touches this rectangle has a planar solution at that point. For example, the entire branch of Lyapunov orbits is planar, so the entire line which represents the Lyapunov orbits touches the gray rectangle. Planar orbits are trivially symmetric about the $x-y$ plane. Solution $B(V,BF)$ is symmetric about the $x-y$ plane but nonplanar. As a visual cue we have depicted it lying in the same plane as the gray rectangle but not touching the gray rectangle. We emphasize that, even though the various visualization aids are in the proper physical position with respect to each other, the bifurcating branches themselves are only schematic. The relative positions of the various solution branches should not be interpreted as signifying any physical property of the solutions, other than those discussed above.

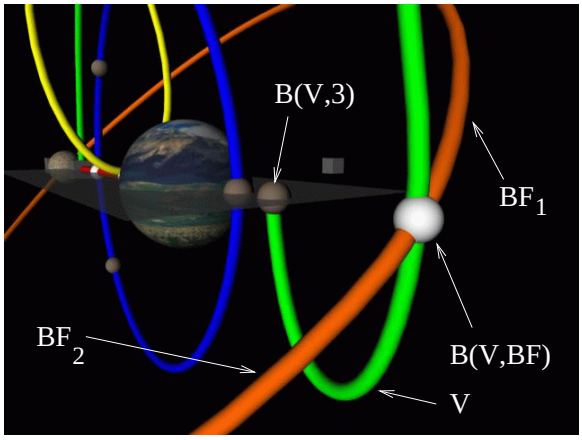

Figure 5: A close-up view of the bifurcation diagram in Figure 4. Here we can see more clearly the bifurcation points $B(V,BF)$ and $B(V,3)$ and the two legs of the branch of Backflip orbits. The bifurcation point $B(V,BF)$ is placed outside the rectangle because the orbit is not planar. Instead we have drawn $B(V,BF)$ in the plane of the rectangle to indicate that the orbit is symmetric with respect to the $x-y$ plane. The two legs BF_1 and BF_2 correspond to the Class 1 and Class 2 families of Backflip orbits (See Figures 10 and 11.) Bifurcation point $B(V,3)$ lies in the rectangle to indicate that the bifurcating orbit is planar. Specifically, $B(V,3)$ is a reverse period-doubling bifurcation.

There are five families of periodic solutions illustrated in Figure 4. On the branch of Lyapunov orbits there are two bifurcations. The first bifurcation from the Lyapunov family gives rise to the branch of Halo orbits labelled with an "H" (see Figure 7). The second bifurcation from the Lyapunov family yields the branch of orbits labelled with an "A" (see Figures 8). We call the solutions on this branch the "Axial" orbits. On the curve of Vertical orbits, labelled by a "V", (see Figure 9) there

[1] In this paper we reserve the terms *bifurcation point* and *bifurcation orbit*, when not further qualified, for transcritical and pitchfork bifurcations, excluding period-doubling, torus, and subharmonic bifurcations.

is a bifurcation that also gives rise to the branch of orbits labelled by an "A". Thus the family of Axial orbits forms a connection between the Lyapunov and Vertical families. The second bifurcation from the branch of Vertical orbits produces the branches labelled "BF_1" and "BF_2" that represent the "Backflip" orbits (see Figures 10 and 11). Figure 5 gives a closer view of this bifurcation point, labelled $B(V, BF)$. In general, we denote the bifurcation point that connects a branch labelled X and a branch labelled Y by $B(X, Y)$. We use the same notation whether we refer to a "bifurcation point" (when the bifurcation is shown on a bifurcation diagram) or a "bifurcation orbit" (when the bifurcation is shown as a physical solution). If we do not pursue a branch in this paper then it is labelled with a number instead of a letter, and the bifurcation point is colored brown. For example, there is a brown-colored bifurcation point labelled $B(V, 3)$ at the end of the branch of Vertical orbits, representing a reverse period-doubling bifurcation to a branch of planar solutions. (When approaching $B(V, 3)$ along this branch of planar solutions, which is not further discussed here, the point $B(V, 3)$ will appear as a regular period-doubling bifurcation.)

We now examine the shapes of the periodic orbits associated with the various branches, beginning with the planar Lyapunov orbits shown in Figure 6. Here and in Figures 7-10 we show both a family of orbits and the bifurcation diagram, with an arrow indicating the relevant branch. The orbits are depicted in the barycentric rotating frame. The gray disk in these figures lies in the $x - y$ plane, centered at the barycenter with radius equal to the Moon's orbit radius R. As a visualization aid we show bifurcation orbits as thickened tubes. The color of the bifurcation orbit indicates the color of the branch to which it connects, if we pursue that branch; otherwise the bifurcation orbit is colored brown. The first bifurcation orbit on the Lyapunov branch, labelled $B(L, H)$ gives rise to the well-known Halo orbits. Accordingly, the thick blue curve labelled $B(L, H)$ in the plane of the Lyapunov orbits is the orbit from which the Halos bifurcate. The second bifurcation orbit on this branch, shown as a thick yellow tube labelled $B(L, A)$, represents the bifurcation orbit to the family of Axial orbits shown in Figure 8. The family of Lyapunov orbits terminates in collisions with the primary bodies.

Figure 7 shows a selection of Northern Halo orbits [5, 21, 35]. To reduce clutter in the diagram, we have only plotted the Northern Halo orbits and not the Southern Halo orbits. The Northern and Southern families of Halo orbits are related through the symmetry $z \to -z$. In Figure 7 the upper left diagram shows the Halo orbits up to a brown bifurcation orbit $B(H, 1)$, whose bifurcating orbits we do not pursue here. (See [14, 48] for details on this branch.) The upper right diagram in Figure 7 begins where the upper left diagram ends. It shows the northern Halo orbits from the bifurcation $B(H, 1)$ up to the second bifurcation $B(H, 2)$ which gives rise to a branch of planar solutions, also not shown here. As the bifurcation diagram indicates, the Halo branch can be continued past the bifurcation to the planar solutions, giving rise to the symmetry-related branch of southern Halos. Accordingly, the branch of Halo orbits in the bifurcation diagram is a loop.

The Axial orbits are shown in Figure 8. We call this family of orbits the Axial orbits, because each orbit is axially symmetric about the x-axis under the transformation $y \to -y$, $z \to -z$, $t \to -t$. The thick red curve $B(L, A)$ is the bifurcation orbit connecting the Lyapunov branch with the Axial branch. The thick green orbit $B(V, A)$, symmetric across the $x - z$ plane, is the bifurcation orbit connecting the Vertical branch and the Axial branch. There is a second symmetry-related family not shown here, and the whole branch of orbits forms a loop as shown in Figure 4. Some of the orbits on the "A" branch were plotted in Zagouras and Kazantzis [58] for $\mu = 0.00095$. These orbits were also computed by Gómez and Mondelo [32] for the Earth-Moon system.

We now turn our attention to the Vertical orbits, shown in Figure 9. In this family there are three bifurcation points beyond L_1, indicated by the tubes labelled $B(V, A)$, $B(V, BF)$ and $B(V, 3)$. The yellow tube $B(V, A)$ represents the bifurcation orbit to the family of Axial orbits. As can be seen, the Vertical orbits grow to encompass the Earth. The orange, nearly-planar orbit $B(V, BF)$ corresponds to the bifurcation point $B(V, BF)$ in Figures 4-5 and represents the bifurcation to the family of Backflip orbits. The Vertical family terminates in a reverse period-doubling bifurcating

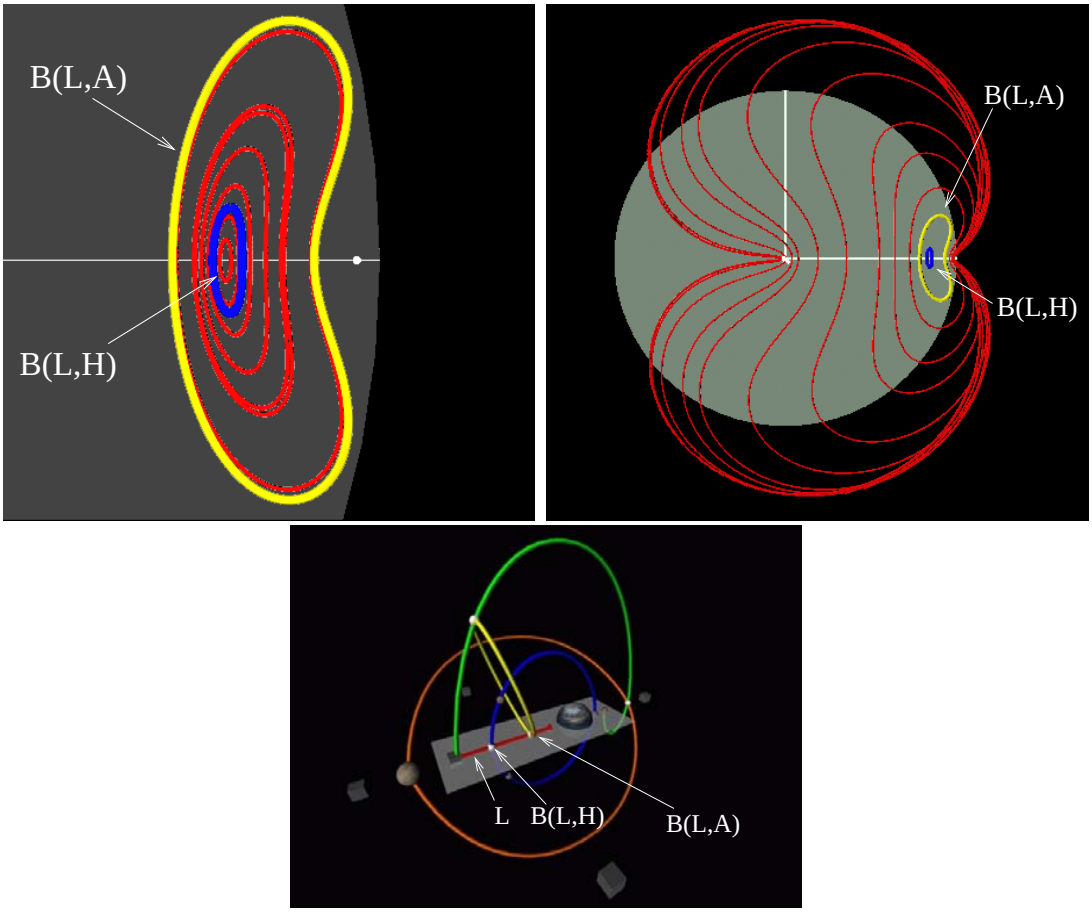

Figure 6: The family of planar Lyapunov orbits. The orbits are depicted in the figures in the barycentric rotating frame. The gray disk lies in the $x-y$ plane, centered at the barycenter with radius equal to the Moon's orbit radius R. The orbits emanate from L_1 on the x-axis. The figure on the upper left shows the two bifurcation orbits in this family. The small white ball at the x-axis represents the Moon, drawn to scale. The thick blue tube labelled $B(L,H)$ represents the first bifurcation orbit to the family of Halo orbits in Figures 7. The first bifurcation orbit has a y amplitude of $0.0559548\ R = 21509$ km and has a period of $2.74298 = 0.436559\ P_{EM}$. The thick yellow tube labelled $B(L,A)$ represents the second bifurcation orbit to the family of Axial orbits shown in Figure 8. The second bifurcation orbit has a y amplitude of $0.250569R = 96319$ km and a period of $3.95007 = 0.628673\ P_{EM}$. The figure on the upper right shows the continuation of the family of Lyapunov orbits beyond the second bifurcation, terminating in collisions with the primaries.

orbit $B(V,3)$, corresponding to the point $B(V,3)$ in Figure 5, where the Vertical branch connects to a branch of planar solutions. The doubly-symmetric Vertical solutions are described in Bray and Goudas [4] and Zagouras and Kazantzis [58].

The second and third bifurcation points on the branch of Vertical solutions can be seen more clearly in Figure 5. Two legs of the branch of Backflip orbits, BF_1 and BF_2, arise from the bifurcation orbit $B(V,BF)$. The family of orbits corresponding to the BF_1 branch are shown in Figures 10 and 11. We refer to the orbits on the BF_1 and BF_2 branches as "Backflip" orbits, named after the Backflip maneuvers described in [56]. Gómez and Mondelo [32] also computed a family of backflip orbits for the Earth-Moon system, following a period-doubling bifurcation.

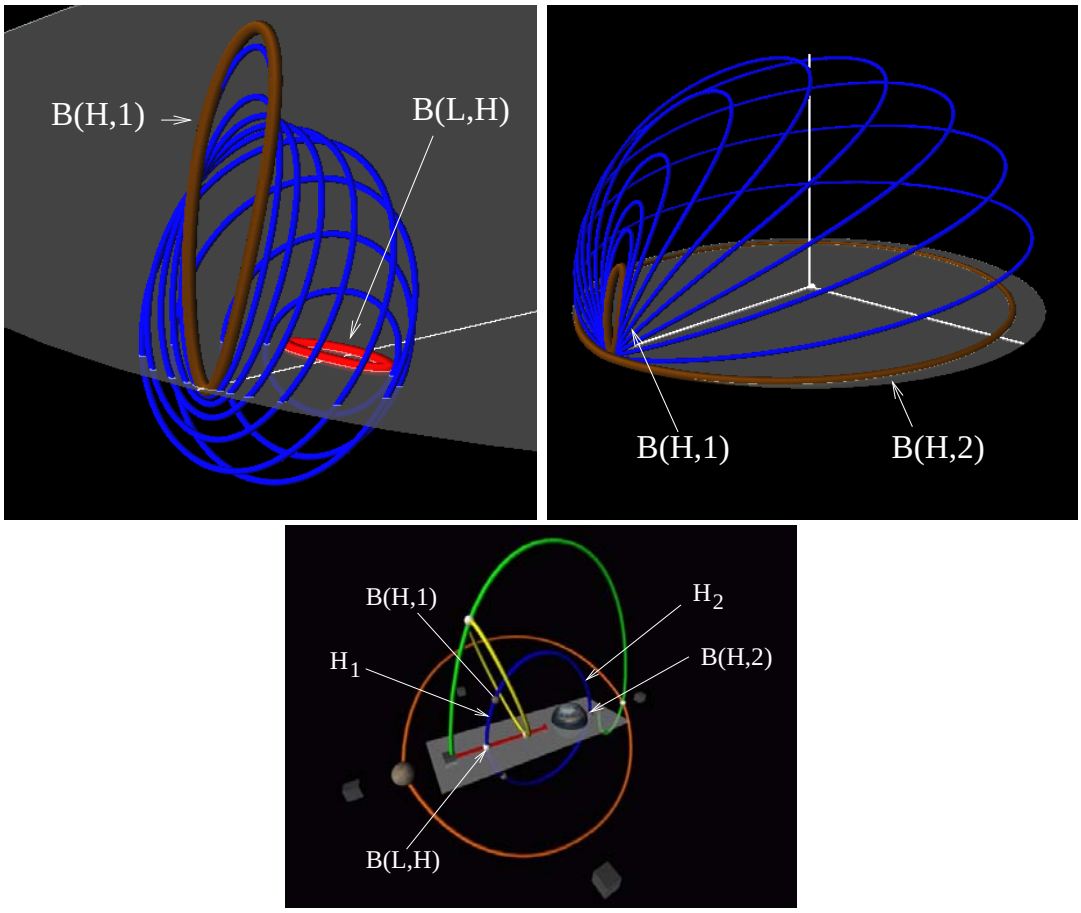

Figure 7: The family of Northern Halo orbits. The upper left figure shows the Halos near the planar bifurcation orbit. The thick red orbit labelled $B(L,H)$ is the Lyapunov orbit from which the Halo orbits bifurcate. The thick brown orbit $B(H,1)$ corresponds to the next bifurcation point on the branch of Halo orbits. The z-amplitude of the $B(H,1)$ orbit is 0.287 R = 110323 km. The orbits in the upper left figure correspond to the part of the bifurcation diagram labelled as "H1". The upper right figure represents the collection of Halo orbits from the bifurcation orbit $B(H,1)$ up to the final bifurcation point $B(H,2)$. The brown curve $B(H,2)$ that encompasses the Earth is a bifurcation orbit that gives rise to a branch of planar orbits not shown here. Once the family passes through $B(H,2)$, it becomes the symmetry-related branch of Southern Halo orbits. Hence, the blue branch of Halo orbits in Figure 4 is a loop. The orbits in the upper right figure are found in the part of the bifurcation diagram labelled as "H2".

Each Backflip orbit consists of two arcs, one above the Earth-Moon orbit plane and one below the orbit plane. The orbits on branch BF_2 are reflections across the $x-y$ plane of the orbits on branch BF_1. We refer to the orbits on branch BF_1 as the Class 1 Backflip orbits, and those on branch BF_2 as the Class 2 Backflip orbits. The two classes BF_1 and BF_2. are related through the symmetry $z \rightarrow -z$.

The Backflip orbits vary smoothly along the branch portions BF_1 and BF_2. However, it is useful to identify five "phases" along each of these branch portions. The first phase of the family of Class 1 Backflip orbits begins at the bifurcation from the Vertical family with both the Northern and Southern arcs near the Earth-Moon orbit plane. Thereafter, as the upper left figure in Figure 10 shows, the z-amplitude of the Northern arc increases to a maximum value close to R. Meanwhile the Southern arc remains near the Earth-Moon orbit plane and moves outward. In the second phase,

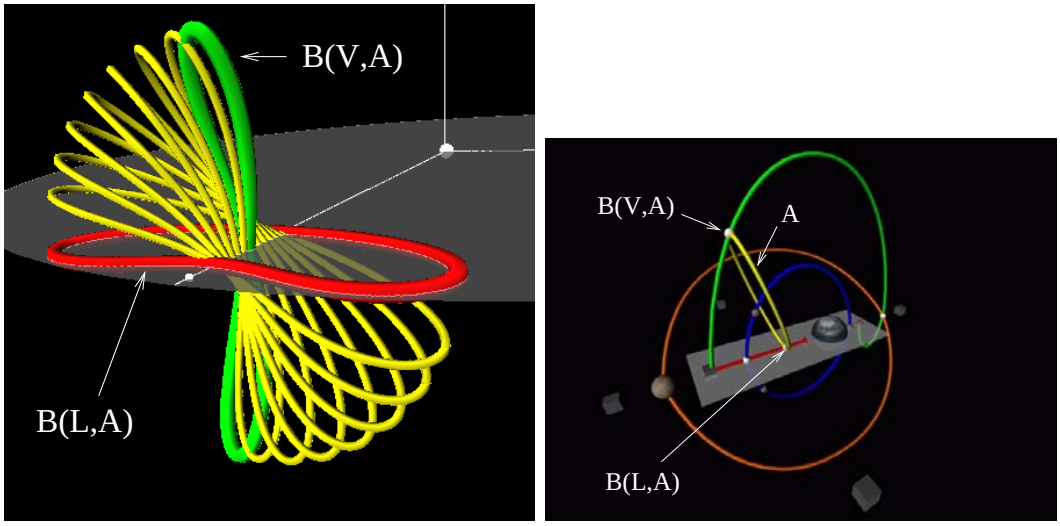

Figure 8: A branch of Axial (axially symmetric) orbits connecting the Lyapunov and Vertical orbits. The thick red curve $B(L, A)$ is the bifurcation orbit connecting the Lyapunov branch with the Axial branch. The thick green orbit $B(V, A)$, symmetric across the $x - z$ plane, is the bifurcation orbit connecting the Vertical branch and the Axial branch. The other yellow curves are a representative collection of the orbits that connect these two bifurcation orbits. The periods of the Axial orbits in the Earth-Moon system lie between 0.629 P_{EM}, where the family connects with the Lyapunov orbits, and 0.647 P_{EM}, where the family connect with the Vertical orbits. There is a second symmetry-related branch not shown here which consists of these above orbits reflected across the $x - z$ plane. Accordingly, the whole branch of orbits forms a loop as shown in Figure 4. The part of the bifurcation diagram where these orbits are found is labelled as "A".

depicted in the upper right figure of Figure 10, the z-amplitude decreases from the maximum to a local minimum value of 0.6465 R. In this second phase the Southern arc moves downward, away from the Earth-Moon orbit plane. In the third phase, depicted in the upper left figure of Figure 11, the z-amplitude of the Northern arc again increases to a value close to R, while the z-amplitude of the Southern arc grows to 2.279 R. In the fourth phase, shown in the upper right figure of Figure 11, the Northern arc drops toward the Earth-Moon orbit plane, while the z-amplitude of the Southern arc decreases. In the final phase, shown in the bottom figure of Figure 11, the Northern arc remains near the $x - y$ plane and extends further outward from the Earth, while the z-amplitude of the Southern arc again increases. The Backflip family terminates in a collision with the Moon.

The transitions between the phases in the Backflip family correlates in part with changes in the Jacobi integral and the minimum distance to the Moon over the course of the branch. For example, near the juncture between phases 1 and 2, the minimum distance to the Moon reaches a local minimum value of 0.006 R = 2275.641 km. Near the juncture between phases 2 and 3, the Jacobi integral achieves a local maximum value of 2.53169. Near the juncture between phases 3 and 4, the Jacobi integral has an inflection point. Near the juncture of phases 4 and 5, the Jacobi integral achieves a local minimum value of -0.932750.

The third bifurcation point from the branch of Vertical solutions, $B(V, 3)$, is a reverse period-doubling bifurcation. Because the bifurcation orbit $B(V, 3)$ is planar, we have drawn bifurcation point $B(V, 3)$ inside the gray rectangle.

The families of periodic orbits we have described exhibit some interesting symmetries. For the N-body problem, the Mirror Theorem [52] states that an orbit is periodic if a mirror configuration occurs at two distinct epochs. This is not a necessary condition for periodicity, but the Mirror

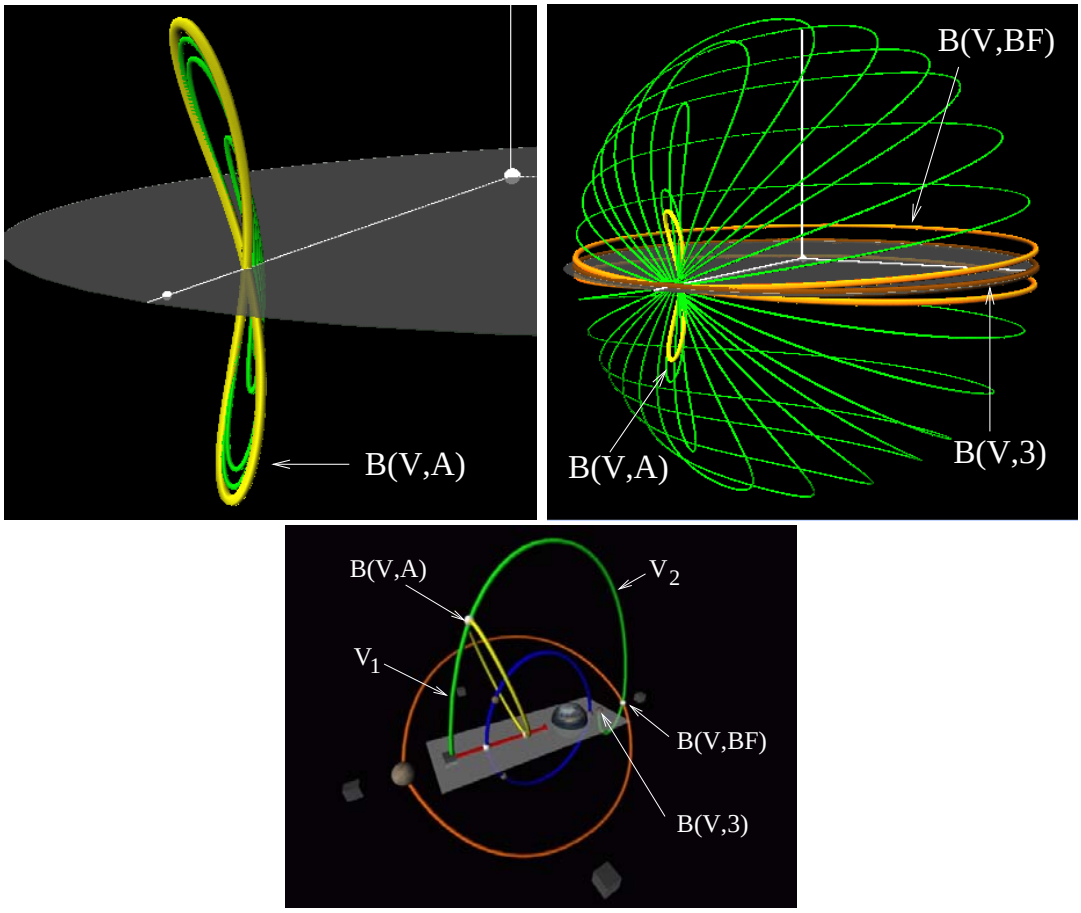

Figure 9: The family of Vertical orbits. The orbits at the three bifurcation points in the family beyond L_1 are shown as thick curves. The upper left figure shows the bifurcating orbit $B(V, A)$, colored yellow. The Axially Symmetric orbits shown in Figure 8 bifurcate from this orbit. The white sphere near the origin of this barycentric system represents the Earth and the white sphere on the positive x-axis represents the Moon, both drawn to scale. The orbits in the upper left figure correspond to the part of the bifurcation diagram labelled as "V1". The orbits in the upper right figure are found in the part of the bifurcation diagram labelled as "V2". The upper right figure represents the collection of Vertical orbits from the bifurcation orbit $B(V, A)$ up to the final bifurcation orbit $B(V, 3)$. The bifurcation orbit $B(V, BF)$, colored orange, encompasses the Earth and lies close to the $x - y$ plane. The Backflip orbits shown in Figures 10 and 11 bifurcate from this orbit. The third bifurcating orbit $B(V, 3)$, colored brown, corresponds to a reverse period-doubling. The orbit is colored brown to indicate that the branch bifurcating from this orbit is not depicted in this paper.

Theorem has been a effective tool for computing periodic solutions near collinear libration points. Robin and Markellos [50] noted that in the CR3BP there are only two types of mirror configurations. In the "P" configuration, the orbit crosses the $x - z$ plane orthogonally; in the "A" configuration, the orbit crosses the x axis orthogonally. Due to symmetries of the CR3BP, an orbit with a point in the P configuration is symmetric across the $x - z$ plane, whereas an orbit with a point in the A configuration is axially symmetric. In Howell [35] and Howell and Campbell [38], periodic orbits were determined by a two-point boundary value problem where each boundary condition describes a P configuration. In the present study we do not exploit the Mirror Theorem in the definition of the boundary conditions. It happens that all of the solutions presented here possess points in the P

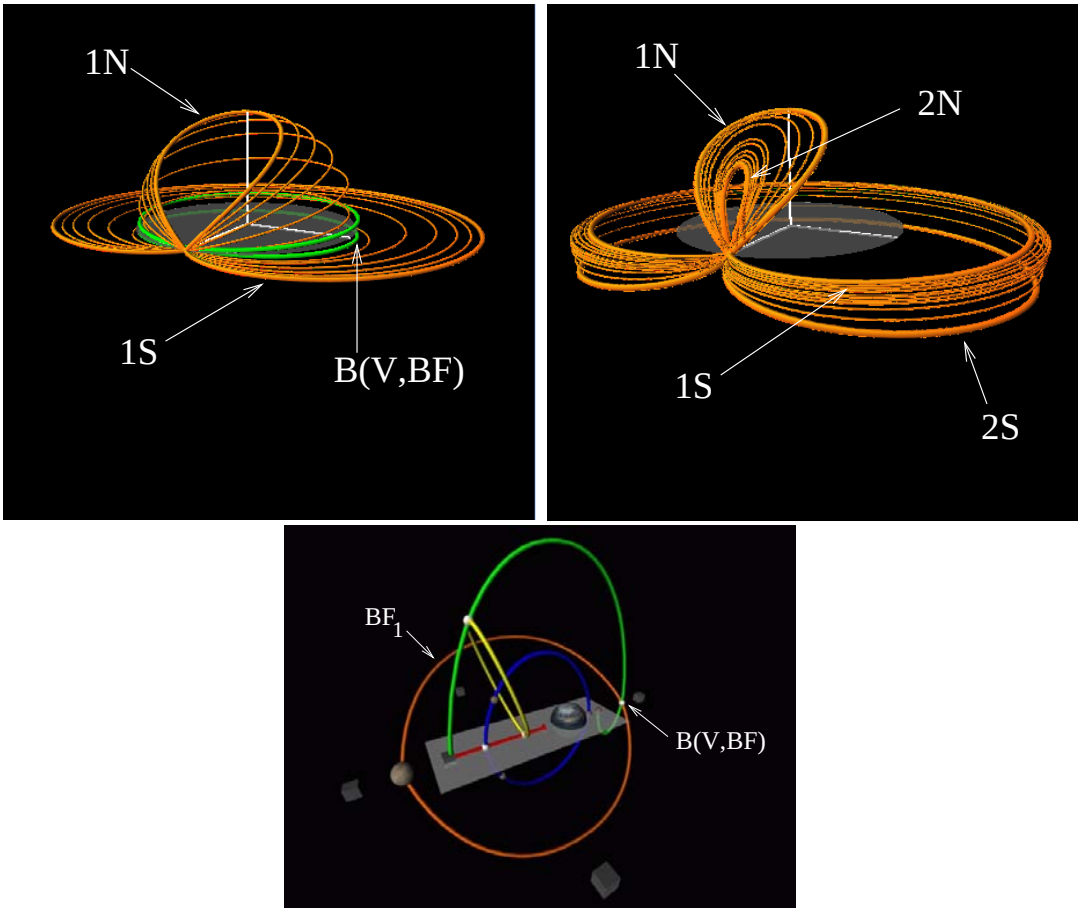

Figure 10: This figure and Figure 11 depict the changes in the Class 1 Backflip orbits along branch BF_1. The upper left figure shows the first phase of the Class 1 family. The family begins at the green tube labelled $B(V, BF)$, representing the bifurcation from the Vertical branch. Thereafter in phase 1 the northern arc of the Backflip orbits increases in amplitude in the positive z direction, until a maximum amplitude close to R is reached. At the same time the Southern arc remains nearly planar but increases in radius. The end of the first phase is shown by a thickened orange tube whose Northern and Southern arcs are labelled 1N and 1S, respectively. However, this tube does not represent a bifurcation. The second phase of the family, shown in the upper right figure, begins where the first phase in the upper left ends. As we follow the Backflip family further, the positive z amplitude of the Northern arc decreases to a value 0.6465 R. At the same time the Southern arc moves further downward, away from the orbit plane of the primaries. The thick orange tube in the upper right figure, with Northern and Southern arcs 2N and 2S, respectively, corresponds to the last orbit in the upper left figure.

configuration (the Halo and Backflip families), points in the A configuration (the Axial family) or both (the Vertical and Lyapunov families). However, as was shown in [14, 48] we can use AUTO2000 to detect families of periodic solutions that possess neither of these types of configurations.

6 ROTATING AND INERTIAL COORDINATES

In Section 3 we defined the barycentric rotating coordinate system. It is convenient to study the CR3BP in rotating coordinates because the equations of motion are time-independent in that frame,

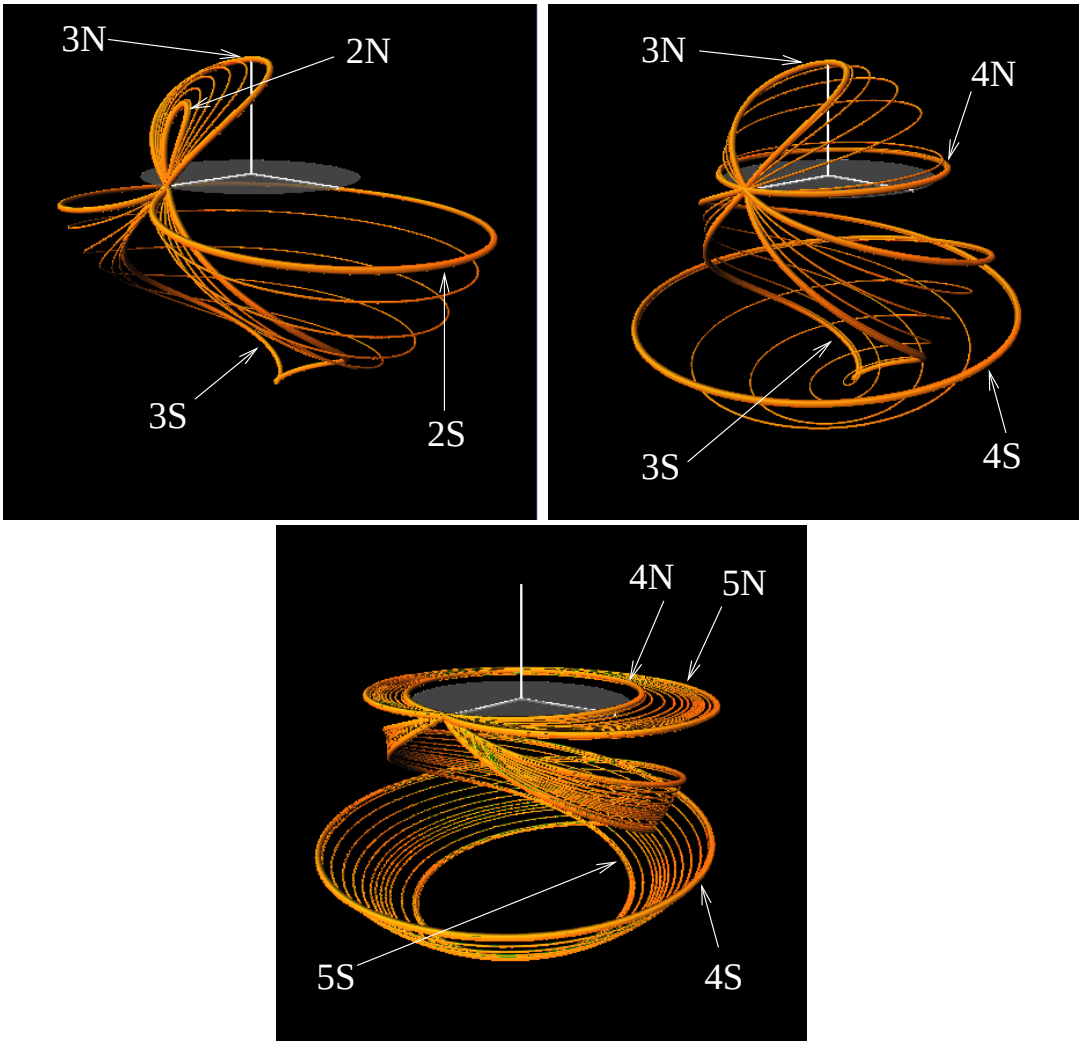

Figure 11: Continuation of the branch of Class 1 Backflip orbits. In the upper left figure, the third phase begins where the second phase in the upper right figure in Figure 10 ends. In the third phase the Northern arc increases in z-amplitude until a maximum amplitude close to R is achieved by the orbit with Northern and Southern arcs 3N and 3S, respectively. In this phase the Southern arcs extend southward until a negative z-amplitude of 2.279 R is reached at the cusp in arc 3S. In the fourth phase, the z-amplitude of the Northern arc decreases toward zero. Meanwhile the Southern arc remains far below the Earth-Moon orbit plane. The fourth phase ends with the orbit with Northern and Southern arcs labelled 4N and 4S. In the final phase, shown in the bottom figure of Figure 11, the Northern arc remains near the $x-y$ plane and extends further outward from the Earth, while the z-amplitude of the Southern arc again increases. The Backflip family terminates in a collision with the Moon. The orbit with arcs 5N and 5S is very close to a collision, passing within 0.56 km of the Moon.

which simplifies the analysis. Moreover the rotating coordinate system is a convenient frame in which to view orbits that remain near a libration point. However, for some trajectories in the three-body problem we can gain further insight by viewing the trajectory in an nonrotating frame as well as the rotating frame. We chose to represent some orbits in an Earth Centered Inertial (ECI) frame in which the axes are aligned, at time $t = 0$, with the axes of the barycentric rotating coordinate system. The angular velocity of the nondimensional rotating frame defined in Section 3 is 1, so the

rotational period of the Earth-Moon system is $P_{EM} = 2\pi$.

An orbit that is periodic in rotating coordinates is, in general, not periodic in inertial coordinates. However, suppose the period P of a solution in rotating coordinates has an $m : n$ resonance with the rotational period P_{EM}; that is, $P/P_{EM} = m/n$ for some integers m and n. Then the trajectory in inertial coordinates is also periodic. (Cf. Hénon [34], Chapter 3.) Specifically, after n Earth-Moon orbit periods, the orbit will complete m periods in rotating coordinates and close in inertial coordinates. This is analogous to the observation that a periodic Keplerian orbit has a repeated ground track if the period in Earth-Centered Inertial coordinates is commensurate with the rotational period of the Earth.

7 APPLICATIONS TO SPACE MISSIONS

The families of periodic orbits described above offer a variety of possible applications to space missions. Due to the fixed positions of L_1 and L_2 along the line between the primaries in the rotating frame, the regions around these libration points provide excellent locations for scientific observation spacecraft and for communication relays [19, 20]. Since 1978, orbits near L_1 and L_2, especially Halo orbits, have been used for scientific missions [24, 42, 51], and there are several future missions planned for these regions [3, 22, 23, 30, 31]. In this paper we focus instead on mission applications of orbits that travel far away from the line between the primaries.

7.1 LYAPUNOV ORBITS

One of the important applications of three-body orbits is to explore geospace, i.e., the fields, plasmas and particles around the Earth [15, 16, 26, 55]. Even within the limitations of planar orbits there are some important mission applications.

Farquhar and Dunham [18] examined the use of orbits with a series of lunar swingbys to observe the Earth's magnetic tail, whose axis is nearly along with the Earth-Sun line. The Earth-Sun line rotates with angular rate $\omega_{SE} = 2\pi/P_{SE}$ in the inertial frame. When viewed in the Earth-Moon rotating frame, the angular rate of the Earth-Sun line is $\omega_{SEM} = \omega_{EM} - \omega_{SE} = 0.9252$, and the period of rotation is $P_{SEM} = 2\pi/\omega_{SEM} = 1.0808\ P_{EM} = 6.7909$. If an orbit has a period that is a multiple of P_{SEM}, then the orbit is periodic in the Earth-Sun rotating frame.

Using AUTO2000, it is straightforward to set parameters that cause the software tool to produce output when it encounters a solution with a specified period. In the class of Lyapunov orbits emanating from L_1, we found two Lyapunov orbits that have periods equal to P_{SEM}. The smaller orbit extends only 0.18 lunar orbit radii beyond the Moon's orbit, and so would be of limited value in exploring the geomagnetic tail. The larger orbit, depicted in Figure 12, extends well beyond the Moon's orbit. In inertial coordinates the orbit appears as a sequence of ellipses, where the line of apsides is rotated by the lunar swingbys at a rate equal to the rotational rate of the Earth-Sun line. If the initial orientation of line of apsides is chosen to lie along the Sun-Earth line, the orbit may be used to monitor the Earth's magnetic tail. Alternatively, if the line of apsides initially points toward the Sun then the orbit can be used to monitor the solar wind. This particular orbit is an Egorov class orbit [18]. If the initial orientation of the line of apsides is chosen to lie along the Sun-Earth line then the orbit can be used to observed the Earth's geomagnetic tail or to observe the solar wind. Unfortunately, at closest approach to the Moon the orbit in Figure 12 would lie 68 km below the surface of the Moon, so the orbit is not useful for mission applications. In fact, Farquhar and Dunham considered the orbit illustrated in Figure 12, and showed that orbits with Double Lunar Swingbys (DLSs) are far more promising for the exploration of the geomagnetic tail

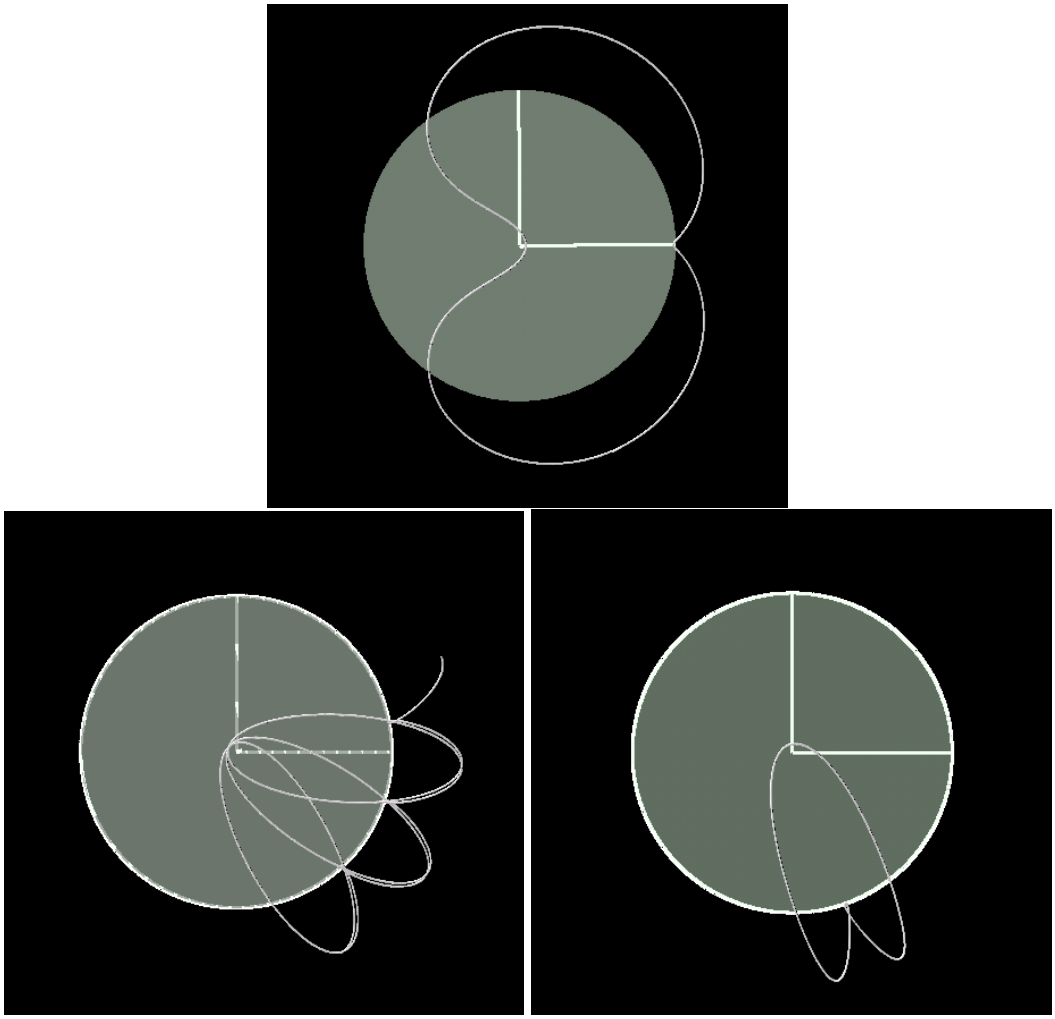

Figure 12: An orbit that tracks the Sun. This Lyapunov orbit has a period equal the period of rotation of the Earth-Sun line in the rotating frame. In this orbit a series of lunar swingbys rotate the line of apsides of the orbit to follow the Sun-Earth line. In this, and in the following figures, we draw the orthogonal axes with length equal to the Moon's orbit radius. We also draw a gray disk with radius equal to the Moon's radius to indicate the Moon's orbit plane. The orbit is displayed in rotating coordinates in the top figure and in ECI coordinates on the bottom left figure. In all figures drawn in inertial coordinates, we also draw the Moon's orbit. The orbit has been propagated for three periods in the ECI frame to demonstrate the rotation of the line of apsides. At closest approach the orbit is 1670 km from the Moon's center, or about 68 km beneath the Moon's surface, making it useless for practical space missions. The figure at the bottom right shows the orbit in an Earth-centered frame that rotate with the Earth-Sun line, and the x-axis points toward the Moon at the initial time.

[18]. (See also [16, 55].) Nevertheless, using AUTO2000 we were able to readily identify candidate orbits for observation of the geomagnetic tail. In this study we have only considered families of orbits emanating from the libration point L_1 between the Earth and the Moon. If we were to perform continuation starting with another family of orbits, we should be able to find more periodic DLS orbits to follow the Sun-Earth line.

Another area of application of three-body orbits is the observation of Coronal Mass Ejections (CMEs) from the Sun. SOHO has been used for several years to observe CMEs. However, as we

remarked above, Halo orbit missions have been restricted in size to simplify communications. As a consequence, the Halo orbits currently in use remain far from the Sun. The Lyapunov orbits in the Sun-Earth system offer an alternative to the Halos as a location from which to observe the Sun-Earth interaction. As can be seen in Figure 6, Lyapunov orbits can be found that pass much closer to the Sun, and extend a significant distance orthogonal to the Sun-Earth line in the $x - y$ plane. However, to offer regular coverage near the Sun-Earth line it would be necessary to insert many spacecraft along the same Lyapunov orbit. Other, similar families of orbits that have been considered for this type of application are Distant Retrograde Orbits about the Earth and Earth Return Orbits emanating from L_2 [27, 28, 40, 45, 46].

7.2 VERTICAL ORBITS

For many space missions it is necessary to travel beyond the orbit plane of the primaries. For missions that observe fields, plasmas and particles, travelling beyond the ecliptic plane permits the spacecraft to sample a broader region of space. For telescopes that observe in the infrared range, it would be extremely valuable for the orbit to extend well beyond the ecliptic plane where the zodiacal dust is concentrated [33]. The large Vertical orbits shown in Figure 9 may be useful for both of these purposes. Because orbits in the Vertical family provide a view of the poles of one or both primaries, they might be useful for polar science missions [25]. For example, an orbit such as the one shown in Figure 13 curves over the Moon's poles and so allows for extended observations of the Moon's polar regions. An analogous orbit in the Earth-Sun system would allow for extended observations of the Earth's poles.

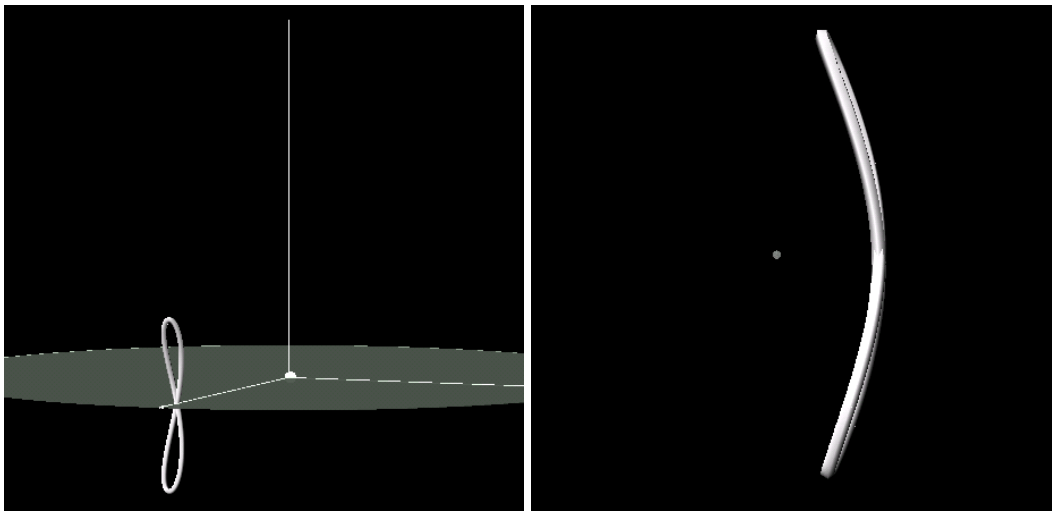

Figure 13: An example of a Vertical orbit displayed in rotating coordinates. This particular orbit is the bifurcation point from which the Axial orbits in Figure 8 arise. This orbit has a period equal to 0.625 P_{EM}. The z-amplitude of this orbit is 0.240 $R = 92250$ km. The figure on the right gives a close-up view of the orbit, where the small gray ball represents the Moon, drawn to scale. Because the orbit bends over the Moon's poles, it offers opportunities to observe the lunar polar regions.

A larger member of the Vertical family, such as the one shown in Figure 14, extends over the poles of the larger primary. From Figure 14 we see that this particular orbit, with a period equal to one Earth-Moon orbit period, is close to being a circular, polar orbit. An analogous orbit in the Sun-Earth system could be used to observe the Sun's polar regions, and because its period equals the Earth-Moon orbit period it would return to the vicinity of the Earth once a year.

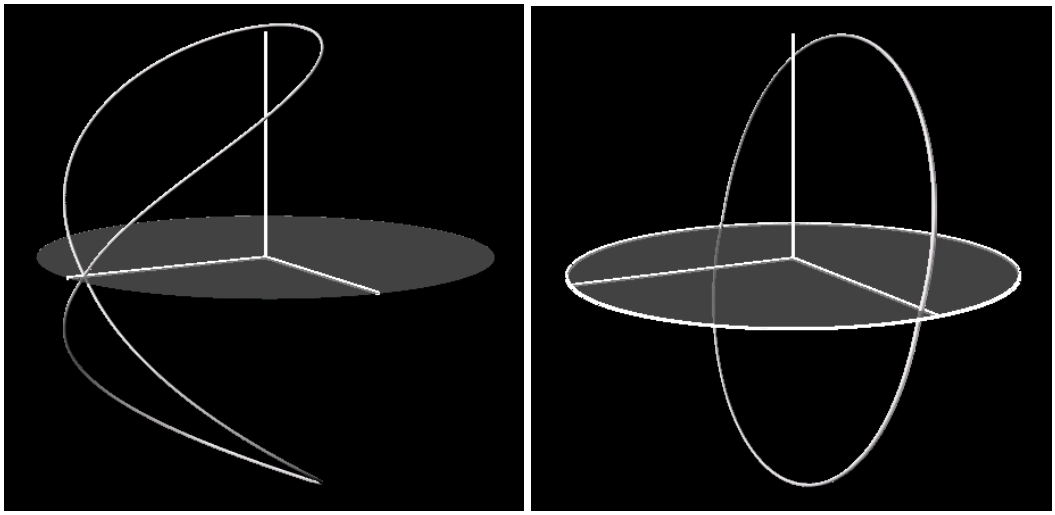

Figure 14: A second example of a vertical orbit displayed in rotating coordinates on the left and in ECI coordinates on the right. This orbit has a period equal to P_{EM}, the Earth-Moon orbit period. The orbit in ECI coordinates is nearly planar and nearly polar.

7.3 AXIAL ORBITS

The Axial orbits shown in Figure 8 form a connection between planar Lyapunov orbits and the Vertical orbits. Indeed each Axial orbit exhibits a combination of the characteristics of the Lyapunov and the Vertical families. One could consider using an Axial orbit in the Sun-Earth system much as one might use a Lyapunov orbit to explore the region between the Sun and the Earth. However, the fact that the Axial orbits extend out of the orbit plane of the primaries adds an extra dimension to the observations a spacecraft could make. In this sense the Axial orbits are similar to the periodic Halo orbits and the quasiperiodic Lissajous orbits. However, the Axial orbits in the Sun-Earth system share a limitation as the Lyapunov orbits: They cross the x-axis periodically, so Sun interference would make communications between the spacecraft and Earth a challenge.

7.4 BACKFLIP ORBITS

The family of Backflip orbits shown in Figures 10 and 11 may offer special opportunities for the exploration of geospace. We call this family "Backflip" orbits because they are reminiscent of the Backflip maneuver described by Uphoff [56].

The Backflip maneuver is an extension of the concept of a Double Lunar Swingby that Farquhar and Dunham described for planar orbits. A Backflip maneuver consists of a pair of lunar swingbys where the first swingby is designed to send a spacecraft, initially moving in the orbit plane of the primaries, far beyond that plane then back for a second encounter with the Moon. The second lunar swingby is designed to return the spacecraft trajectory to the orbit plane of the primaries. By using a Backflip maneuver, a spacecraft can sample the region beyond the primaries' orbit plane and still remain in the vicinity of the Earth. The Wind mission employed several Backflip maneuvers for this purpose in the Earth-Moon system [27]. A Backflip orbit then consists of a periodic sequence of Backflip maneuvers. In the Sun-Earth system, a Backflip orbit could also make it possible for a space telescope to reduce the effects of the zodiacal dust.

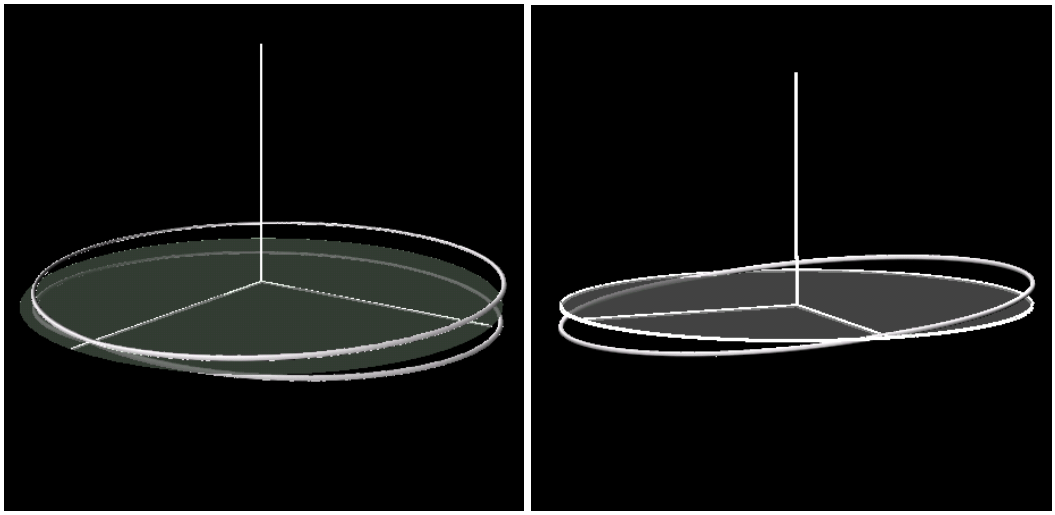

Figure 15: The Backflip bifurcation orbit. This is the same as the orbit $B(V, BF)$ shown in Figure 10. The orbit is displayed here in rotating coordinates on the left and in ECI coordinates on the right. The orbit has been propagated for 4 Earth-Moon orbit periods in the ECI frame. This orbit is doubly symmetric in rotating coordinates. In ECI coordinates the orbit is very close to being a slightly inclined circular orbit whose radius is the same as the Moon's orbit radius. The period of the orbit is 1.002 Earth-Moon orbit periods, so it nearly closes in the ECI frame.

The periods of the Backflip orbits range upward from 1.002 Earth-Moon orbit periods. The bifurcation orbit, where the family of Backflips arises from the Vertical family, is shown in Figure 15. We have extended the family up to its collision with the Moon's surface where the period is 2.286 P_{EM}. Figures 15- 22 show representative members of the Class 1 Backflip orbits from Figure 10 and 11 in both rotating and ECI coordinates. As we noted in Section 5, the branch of Class 1 Backflip orbits can be divided into five phases, where the z-amplitude of the Northern arc of the orbit first increases in phase 1 to a value close to the Moon's orbit radius R, then decreases in phase 2 to a local minimum of $0.6465R$, then increases in phase 3 to a value near R again, then decreases in phase 4 toward zero. In the fifth and final phase the Northern arc remains near the $x - y$ plane and the orbits move outward from the Earth. The five phases are depicted in Figures 10 and 11.

Figure 16 is a representative member of the first phase of Backflip orbits. Because the orbit in Figure 16 has a $4 : 3$ resonance, the orbit is periodic in the inertial frame and closes after 3 Earth-Moon orbit periods. It is not clear that a resonant orbit has any practical advantages over nonresonant orbits. However, the simple, symmetric structure of this orbit in inertial coordinates makes it easier to comprehend.

The orbit in Figure 17, which lies at the junction between phases 1 and 2, has some very interesting properties. This orbit has a $3 : 2$ resonance with the Earth-Moon orbit period. When viewed in inertial coordinates, the orbit is nearly planar. One portion of the orbit is approximately a polar, semicircular arc with radius near the Moon's orbit radius. As a consequence, that portion of the orbit is traced out in one-half Earth-Moon orbit period. The remainder of the orbit with $3 : 2$ resonance consists of two segments beyond the Moon's orbit that are close to being linear and radial. Each of these orbit segments is traced out in one-half Earth-Moon orbit period. The nearly circular segment is connected to each of the nearly linear segments by a lunar swingby. While the orbit has a period of 1.5 Earth-Moon orbit periods in the rotating frame, it actually requires 3 Earth-Moon orbit periods to complete one orbit in the inertial frame.

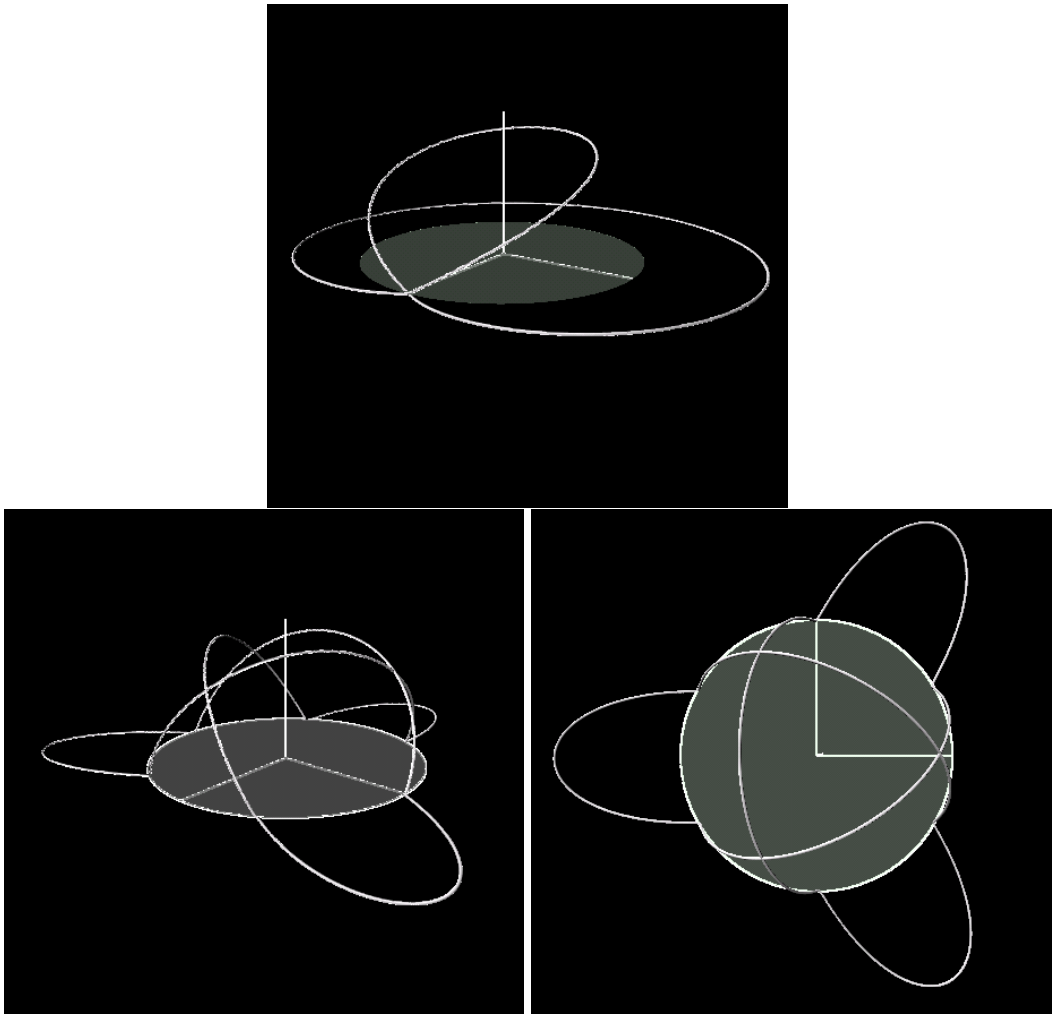

Figure 16: A Backflip orbit with 4 : 3 resonance. This orbit is part of the first phase of Class 1 Backflip orbits. The orbit is displayed in rotating coordinates in the top figure. The bottom figures show the orbit in ECI coordinates, with a skew view on the left and a projection into the $x - y$ plane of the right. The orbit has been propagated for 3 Earth-Moon orbit periods in the ECI frame. This orbit has a period of 4/3 P_{EM}. Therefore the orbit closes in the ECI frame after 3 Earth-Moon orbit periods. This orbit, like those shown in Figures 17- 22, lacks symmetry across the $x - y$ plane.

As we trace the family of Class 1 Backflips further (represented in Figures 15- 22), the maximum z-amplitude initially decreases to a value of $0.646R$, the maximum radius in the plane of the primaries increases, and the minimum distance to the Moon increases. As we trace the family further, the maximum z-amplitude increases again and the near-planar portion of the orbit becomes significantly nonplanar. An orbit such as the one in Figures 20-22 would allow a spacecraft to explore space to a z-amplitude greater than $2R$. As the family of Class 1 Backflips is followed further, the nonplanar portion of the orbit lies entirely below the orbit plane of the primaries. Figure 22 shows the shape of the Backflip orbits just before collision with the Moon's surface.

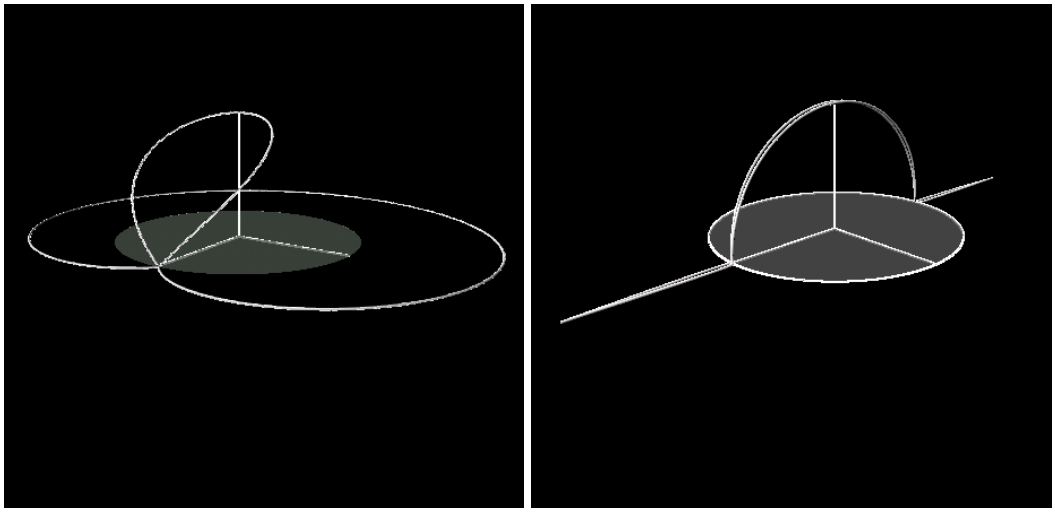

Figure 17: A Backflip orbit with 3 : 2 resonance. This orbit lies at the junction between the first and second phases of the Class 1 Backflips, and corresponds to the orbit with Northern and Southern arcs 1N and 1S shown in Figure 10. The orbit is displayed in rotating coordinates on the left and in ECI coordinates on the right. The orbit has been propagated for 2 Earth-Moon orbit periods in the ECI frame. This orbit has a period equal to 3/2 P_{EM}, and closes after two Earth-Moon orbit periods. It is remarkable that this orbit is nearly planar.

8 CONCLUSION

In this paper we have shown how the numerical continuation methods in AUTO2000 may be applied to the computation of periodic orbits in the Circular Restricted 3-Body Problem (CR3BP). Pseudo-arclength continuation provides a robust method for computing periodic orbits which neither depends on any symmetry properties of the desired solutions nor upon any expansions about the equilibria from which the solution arise. The general theory of numerical continuation does not immediately apply to conservative systems such as the CR3BP. However with the introduction of a unfolding parameter we can reformulate the problem to make the techniques in AUTO2000 applicable. Through the use of a Python script to drive AUTO2000 we are able to compute periodic orbits of arbitrary extent and follow all bifurcating branches. Our focus in this paper has been on the computation and mission applications of a subset of the branches that we have computed for the CR3BP. Other branches of the bifurcation diagram are explored in [14, 48] and references cited therein, where it is shown that there is a rich variety of periodic solutions emanating from the various libration points. Indeed, the families of periodic orbits form connections between the different libration points. Deprit and Henrard [7, 8] in particular described intricate connections between families of periodic orbits in the planar CR3BP.

It is common to compute periodic solutions of the CR3BP in a rotating coordinate system, where the dynamical system is autonomous. However to understand the nature and applicability of solutions that travel far from a libration point, it useful to represent the solutions in an Earth Centered Inertial frame. We have also used a feature in AUTO2000 that allows one to identify members of a family with particular periods. These tools have allowed us to explore the applicability to space missions of members of the Lyapunov, Vertical, Halo and Axially Symmetric branches from L_1. We have paid particular attention to members of the family of "Backflip" orbits and their application to the exploration of geospace. In this study we have identified some physical quantities that correlate with the phase transitions. It would be enlightening to examine in greater detail the

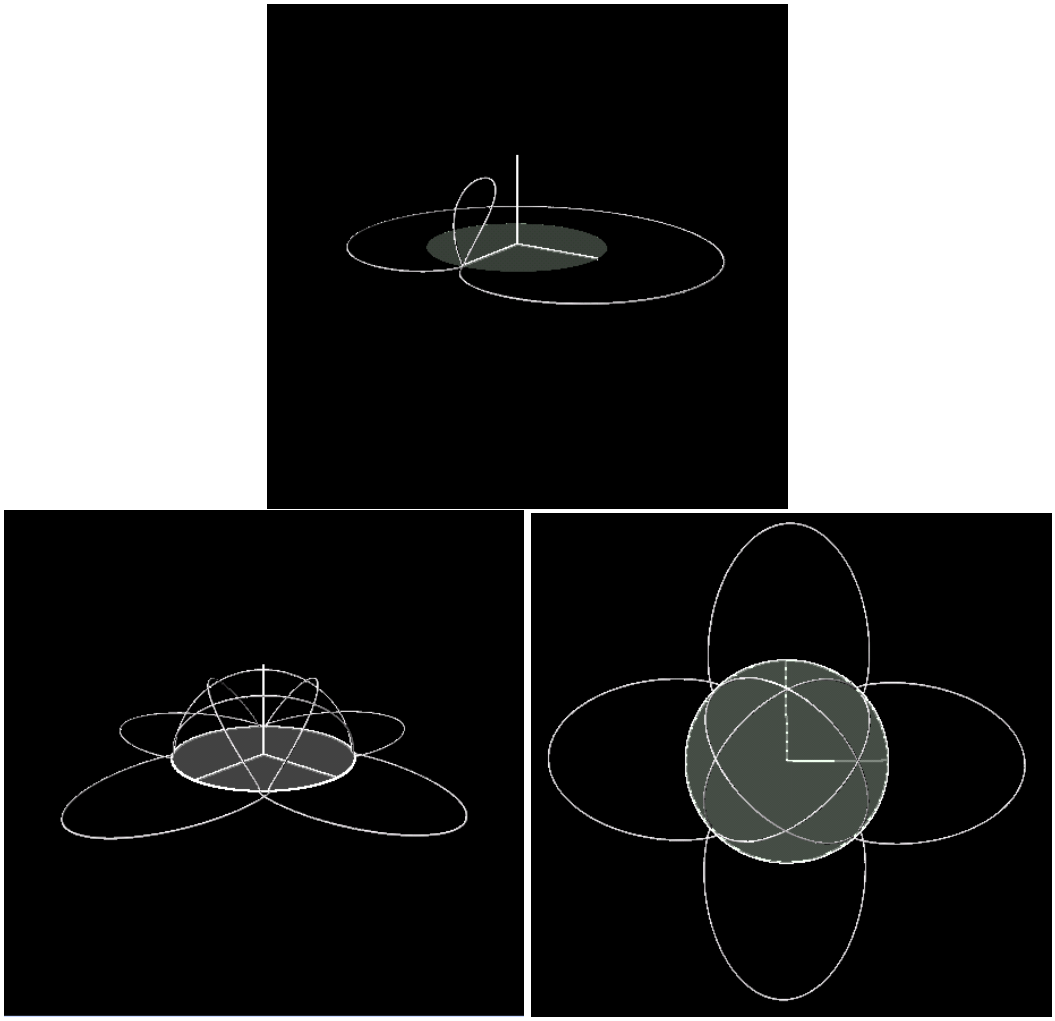

Figure 18: A Backflip orbit with 7 : 4 resonance. This orbit lies in the second phase of the Class 1 Backflips. The orbit is displayed in rotating coordinates in the top figure. The bottom figures show the orbit is ECI coordinates, with a skew view on the left and a projection into the $x - y$ plane on the right.

geometry of the close approach with the Moon, through an examination of the B-plane parameters [17] for example.

We have not addressed stability issues in this paper, although AUTO2000 computes Floquet multipliers and eigenvectors. For example, we found that many Backflip orbits have at least one large Floquet multiplier, indicating instability. Because many Backflip orbits pass close to Moon, it is not surprising that they would be unstable. For a Backflip orbit to be viable for a spacecraft mission, it would be necessary to demonstrate that the orbit can be stabilized using an acceptable fuel budget. Floquet multipliers and eigenvectors can also be used in AUTO2000 to determine stable and unstable manifolds associated with an orbit. Recent work in libration point dynamics has focused on the invariant manifolds associated with the libration points and orbits about them (see, for example, [3, 29, 37]). In future work it would be interesting to use these manifolds to determine efficient ways to insert a spacecraft into one of the orbits discussed in this work.

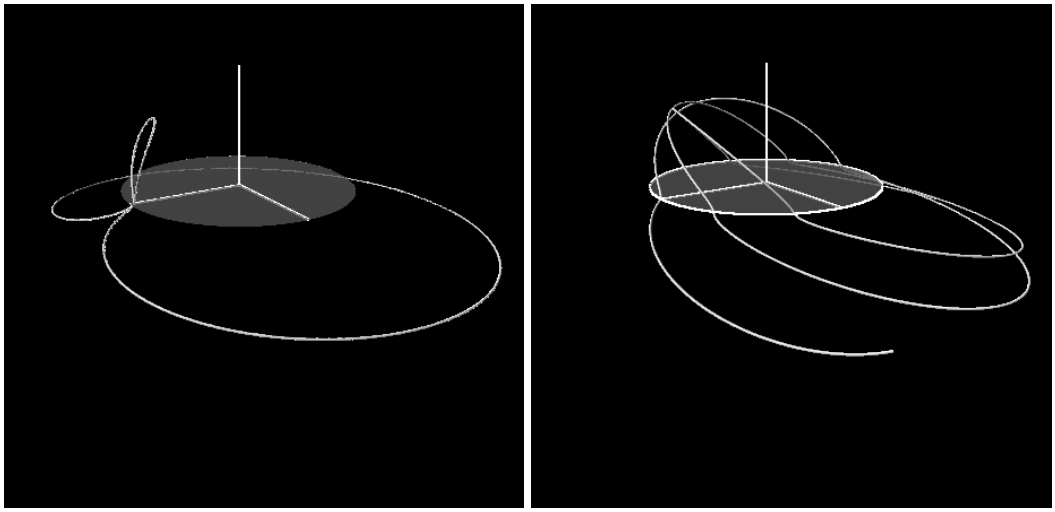

Figure 19: A Backflip orbit with the positive z-amplitude at a local minimum. This orbit lies at the junction between the second and third phases of the Class 1 Backflips, and corresponds to the orbits with Northern and Southern arcs 2N and 2S in Figures 10-11. The orbit is displayed in rotating coordinates on the left and in ECI coordinates on the right. The orbit has been propagated for 3 Earth-Moon orbit periods in the ECI frame. The period of the orbit is 1.902 P_{EM}. Because the orbit does not have a simple resonance, it does not close in a few Earth-Moon orbit periods in the ECI frame.

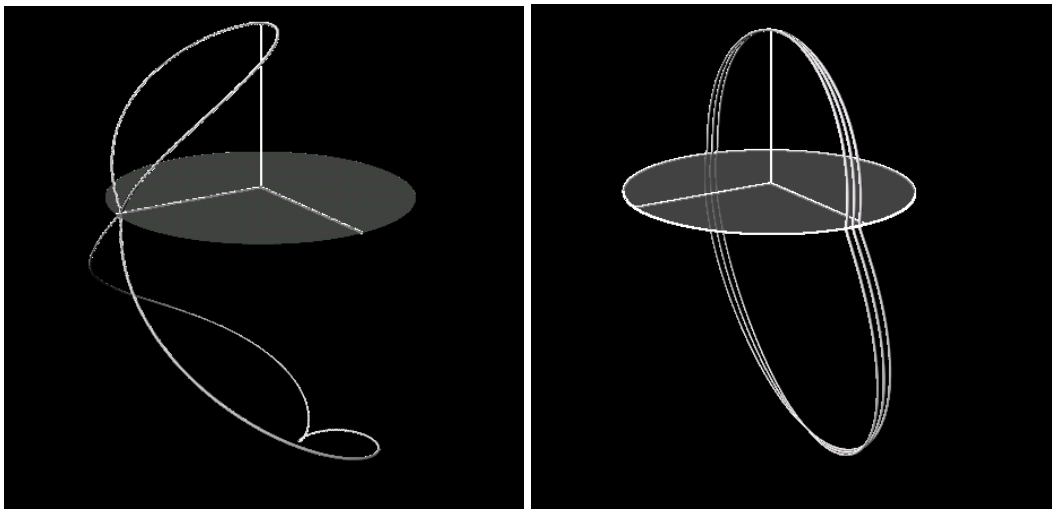

Figure 20: A Backflip orbit where the positive z-amplitude reaches a maximum value very close to R. This orbit lies at the junction between the third and fourth phases of the Class 1 Backflip orbits, and corresponds to the orbits with Northern and Southern arcs 3N and 3S in Figure 11. The orbit is displayed in rotating coordinates on the left and in ECI coordinates on the right. The orbit has been propagated for 3 Earth-Moon orbit periods in the ECI frame. The period of the orbit is 1.992 P_{EM}. The orbit nearly closes in the ECI frame after one Earth-Moon orbit period.

ACKNOWLEDGEMENTS

DJD thanks Chauncey Uphoff, Peter Sharer and Heather Franz for introducing him to the principles and applications of the Backflip maneuver. This work was also inspired in part by the studies of

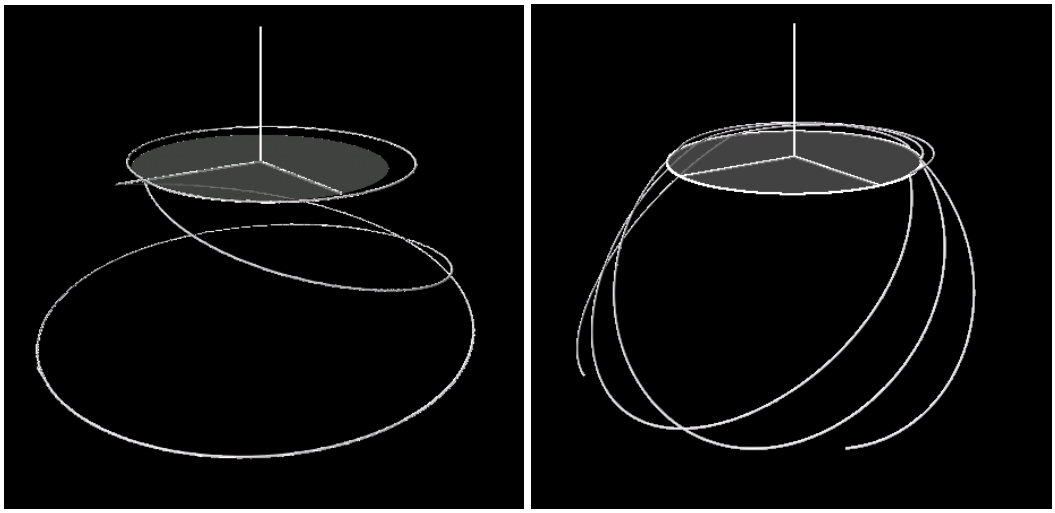

Figure 21: A Backflip orbit where the Northern arc lies approximately in the orbit plane of the primaries. This orbit lies at the juncture of the fourth and fifth phases of Class 1 Backflip orbits, and corresponds to the orbits with Northern and Southern arcs 4N and 4S in Figure 11. The orbit is displayed in rotating coordinates on the left and in ECI coordinates on the right. The orbit has been propagated for 3 Earth-Moon orbit periods in the ECI frame. The Northern arc of the orbit lies very close to the Earth-Moon orbit plane, while the Southern arc extends far below that plane.

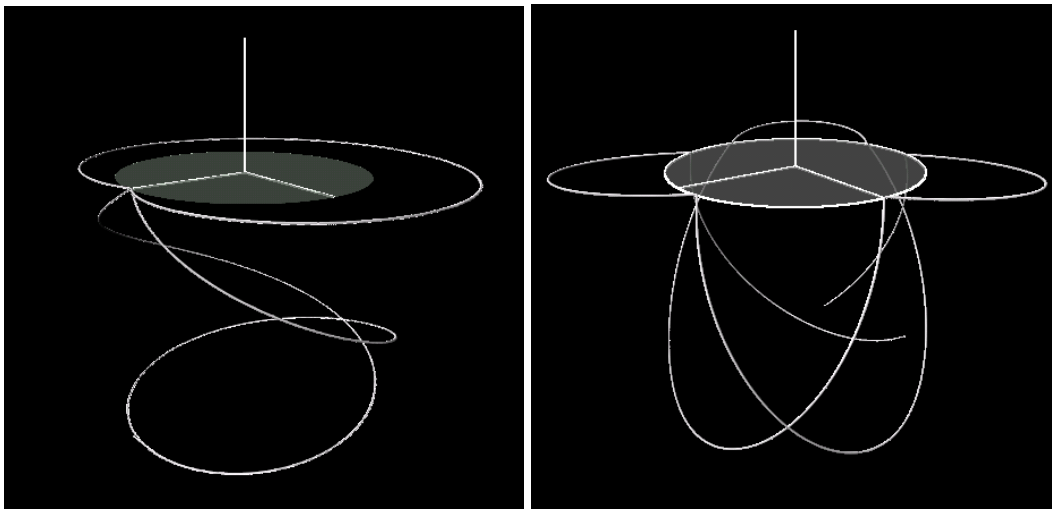

Figure 22: A Backflip orbit near collision with the Moon. This orbit is part of the fifth phase of Class 1 Backflips, and corresponds to the orbits with Northern and Southern arcs 5N and 5S in Figure 11. The orbit is displayed in rotating coordinates on the left and in ECI coordinates on the right. The orbit has been propagated for 3 Earth-Moon orbit periods in the ECI frame. This orbit has a period equal to 2.286 P_{EM} and passes within 0.56 km of the Moon's surface.

"orbital acrobatics" by Dr. David Dunham and his colleagues. Thank you to Dr. Kent Bradford for his constructive comments. The work of EJD and RCP has been partially supported by NSF grant KDI/NCC SBR-9873173. EJD is also supported by NSERC Canada, Research Grant A4274. Our thanks to Christine Thorn for her invaluable assistance with the graphics.

References

[1] E. L. Allgower and K. Georg. Numerical path following. In P. G. Ciarlet and J. L. Lions, editors, *Handbook of Numerical Analysis*, volume 5. North Holland Publishing, 1996.

[2] U. M. Ascher, J. Christiansen, and R. D. Russell. Collocation software for boundary value ODEs. *ACM Trans. Math. Software*, 7:209–222, 1981.

[3] B. T. Barden and K. C. Howell. Fundamental motions near collinear libration points and their transitions. *J. Astronautical Sciences*, 46(4):361–378, 1998.

[4] T. A. Bray and C. L. Goudas. Doubly symmetric orbits about the collinear Lagrangian points. *The Astronomical Journal*, 72(2):202–213, 1967.

[5] J. V. Breakwell and J. V. Brown. The "Halo" family of 3-dimensional periodic orbits in the Earth-Moon restricted 3-body problem. *Celestial Mechanics*, 20:389–404, 1979.

[6] J. M. A. Danby. *Fundamentals of Celestial Mechanics.* Willmann-Bell, 1992.

[7] A. Deprit and J. Henrard. A manifold of periodic orbits. In Z. Kopal, editor, *Advances in Astronomy and Astrophysics*, pages 1–124. Academic Press, 1968.

[8] A. Deprit and J. Henrard. The Trojan manifold - Survey and conjectures. In G. E. O. Giacaglia, editor, *Periodic Orbits, Stability and Resonances*, pages 1–18. D. Reidel Publishing Co., Dordrecht-Holland, 1970.

[9] E. J. Doedel, D. G. Aronson, and H. G. Othmer. The dynamics of coupled current-biased Josephson junctions II. *Int. J. Bifurcation and Chaos*, 1(1):51–66, 1991.

[10] E. J. Doedel, A. R. Champneys, T. F. Fairgrieve, Yu. A. Kuznetsov, B. Sandstede, and X. J. Wang. AUTO97: Continuation and bifurcation software for ordinary differential equations. Available via http://cmvl.cs.concordia.ca, 1997.

[11] E. J. Doedel, H. B. Keller, and J. P. Kernévez. Numerical analysis and control of bifurcation problems: I. *Int. J. Bifurcation and Chaos*, 1(3):493–520, 1991.

[12] E. J. Doedel, H. B. Keller, and J. P. Kernévez. Numerical analysis and control of bifurcation problems: II. *Int. J. Bifurcation and Chaos*, 1(4):745–772, 1991.

[13] E. J. Doedel, R. C. Paffenroth, A. R. Champneys, T. F. Fairgrieve, Yu. A. Kuznetsov, B. E. Oldeman, B. Sandstede, and X. J. Wang. AUTO2000: Continuation and bifurcation software for ordinary differential equations. Available via http://cmvl.cs.concordia.ca, 2000.

[14] E. J. Doedel, R. P. Paffenroth, H. B. Keller, D. J. Dichmann, J. Galán-Vioque, and A. Vanderbauwhede. Computation of periodic solutions of conservative systems with application to the 3-body problem. *Int. J. Bifurcation and Chaos*, 2002. Accepted.

[15] D. W. Dunham and S. A. Davis. Catalog of Double Lunar Swingby orbits for exploring the earth's geomagnetic tail. Technical report, October 1980. Computer Sciences Corporation, CSC/TM-80/6322.

[16] D. W. Dunham and S. A. Davis. Optimization of a multiple lunar-swingby trajectory sequence. *J. Astronautical Sciences*, 33(3):275–288, July-September 1985.

[17] L. Efron, D.K. Yeomans, and A.F. Schanzle. ISEE-3/ICE navigation analysis. *J. Astronautical Sciences*, 33(3):301–323, July-September 1985.

[18] R. Farquhar and D. Dunham. A new trajectory concept for exploring the Earth's geomagnetic tail. *J. Guidance and Control*, 4(2):192–196, March-April 1981.

[19] R. W. Farquhar. The flight of ISEE-3/ICE: Origins, mission history and a legacy. *J. Astronautical Sciences*, 49(1):23–73, 2001.

[20] R. W. Farquhar and D. W. Dunham. Use of libration points for space observatories. In *Observatories in Earth Orbit and Beyond*, pages 391–395. Kluwer Academic Publishers, 1990.

[21] R. W. Farquhar and A. K. Kamel. Quasi-periodic orbits about the translunar libration point. *Celestial Mechanics*, 7:458–473, 1973.

[22] F. Felici, M. Hechler, and F. Vanderbussche. The ESA astronomy missions at L2: FIRST and Planck. *J. Astronautical Sciences*, 49(1):185–196, 2001.

[23] D. Folta, S. Cooley, and K. Howell. Trajectory design strategies for the NGST L2 libration point mission. In *AAS/AIAA Space Flight Mechanics Meeting*, 2001. AAS 01-205.

[24] D. Folta and K. Richon. Libration orbit mission design at L2: A MAP and NGST perspective. In *AIAA/AAS Astrodynamics Specialist Conference*, 1998. AIAA 98-4469.

[25] D. Folta, C. Young, and A. Ross. Unique non-Keplerian orbit vantage locations for Sun-Earth connections and Earth Science Vision roadmaps. In *NASA Goddard Flight Dynamics Symposium*, 2001.

[26] D. C. Folta and S. L. Sauer. ISEE-3 trajectory control utilizing multiple lunar swingbys. In *AAS/AIAA Space Flight Mechanics Meeting*, August 1984. AIAA 84-1979.

[27] H. Franz. Wind lunar backflip and Distant Prograde Orbit implementation. In *AAS/AIAA Space Flight Mechanics Meeting*, 2001. AAS 01-173.

[28] H. Franz. Design of Earth Return Orbits for the Wind mission. In *AAS/AIAA Space Flight Mechanics Meeting*, 2002. AAS 02-170.

[29] G. Gómez, K. S. Koon, M. W. Lo, J. E. Marsden, J. Masdemont, and S. D. Ross. Invariant manifolds, the spatial three-body problem and space mission design. In *AAS/AIAA Astrodynamics Specialist Conference*, 2001. AAS 01-301.

[30] G. Gómez, M. W. Lo, J. Masdemont, and K. Museth. Simulation of formation flight near Lagrange points for the TPF mission. In *AAS/AIAA Astrodynamics Specialist Conference*, 2001. AAS 01-305.

[31] G. Gómez, J. Masdemont, and C. Simó. Lissajous orbits around halo orbits. In *AAS/AIAA Space Flight Mechanics Meeting*, 1997. AAS 97-106.

[32] G. Gómez and J.M. Mondelo. The dynamics around the collinear equilibrium points of the RTBP. *Physica D*, 157:283–321, 2001.

[33] P. Gurfil and N.J. Kasdin. Optimal out-of-the-ecliptic trajectories for space-borne observatories. In *AAS/AIAA Space Flight Mechanics Meeting*, 2001. AAS 01-162.

[34] M. Hénon. *Generating Families in the Restricted Problem*. Springer-Verlag, 1997.

[35] K. C. Howell. Three-dimensional, periodic, 'Halo' orbits. *Celestial Mechanics*, 32:53–71, 1984.

[36] K. C. Howell. Families of orbits in the vicinity of the collinear libration points. In *AIAA/AAS Astrodynamics Specialist Conference*, 1998. AAS 98-4465.

[37] K. C. Howell, B. T. Barden, and M. W. Lo. Applications of dynamical systems theory to trajectory design for a libration point mission. *J. Astronautical Sciences*, 45(2):161–178, 1997.

[38] K. C. Howell and E. T. Campbell. Three-dimensional periodic solutions that bifurcate from Halo families in the circular restricted three-body problem. In *Spaceflight Mechanics*, 1999. AAS 99-161.

[39] S. Ichtiaroglou and M. Michalodimitrakis. Three-body problem: The existence of families of three-dimensional periodic orbits. *Astronomy and Astrophysics*, 81:30–32, 1980.

[40] J. A. Kechichian, E. T. Campbell, M. F. Werner, and E. Y. Robinson. Solar surveillance zone population strategies with picosatellites using Halo and Distant Retrograde Orbits. In *International Conference on Libration Point Orbits and Applications, Aiguablava, Spain*, 2002.

[41] H. B. Keller. Numerical solution of bifurcation and nonlinear eigenvalue problems. In P. H. Rabinowitz, editor, *Applications of Bifurcation Theory*, pages 359–384. Academic Press, 1977.

[42] M. W. Lo, B. Williams, W. Bollman, D. Han, Y. Hahn, J. Bell, E. Hirst, R. Corwin, P. Hong, K. Howell, B. Barden, and R. Wilson. Genesis mission design. *J. Astronautical Sciences*, 49(1):169–184, 2001.

[43] K. R. Meyer. *Periodic Solutions of the N-Body Problem.* Springer Verlag, 1999.

[44] F. J. Muñoz-Almaraz, E. Freire, E. J. Doedel, A. Vanderbauwhede, and J. Galán. Continuation of periodic orbits in conservative and Hamiltonian systems. In preparation.

[45] C. Ocampo. *Trajectory Optimization for Distant Earth Satellites and Satellite Constellations.* PhD thesis, University of Colorado, 1996.

[46] C. Ocampo and G. W. Rossborough. Transfer trajectories for Distant Retrograde Orbiters of the Earth. In *AAS/AIAA Space Flight Mechanics Meeting*, 1993. AAS 93-180.

[47] R. C. Paffenroth and E. J. Doedel. The AUTO2000 command line user interface. In *Proceedings of the 9th International Python Conference*, pages 233–241, March 2001.

[48] R. C. Paffenroth, E. J. Doedel, and D. J. Dichmann. Continuation of periodic orbits around Lagrange points and AUTO2000. In *AAS/AIAA Astrodynamics Specialist Conference*, 2001. AAS 01-303.

[49] W. C. Rheinboldt. *Numerical analysis of parametrized nonlinear equations.* Wiley-Interscience, 1986. University of Arkansas Lecture Notes in the Mathematical Sciences.

[50] I. A. Robin and V. V. Markellos. Numerical determination of the three-dimensional periodic orbits generated from vertical self-resonant satellite orbits. *Celestial Mechanics*, 21:395–434, 1980.

[51] J. Rodriguez-Canabal and M. Hechler. Orbital aspects of the SOHO mission design. In *Orbital Mechanics and Mission Design*, volume 69 of *Advances in the Astronautical Sciences*, pages 347–356, 1989. AAS 89-171.

[52] A. E. Roy. *Orbital Motion.* Adam Hilger, 1988.

[53] R. D. Russell and J. Christiansen. Adaptive mesh selection strategies for solving boundary value problems. *SIAM J. Numer. Anal.*, 15:59–80, 1978.

[54] V. Szebehely. *Theory of Orbits: The Restricted Problem of Three Bodies.* Academic Press, 1967.

[55] K. Uesegi, J. Kawaguchi, S. Ishii, N. Ishii, M. Kimura, and K. Tanaka. Design of Double Lunar Swingby orbits for MUSES-A and GEOTAIL. In *AAS/AIAA Space Flight Mechanics Meeting*, volume 69 of *Advances in the Astronautical Sciences*, August 1984. AAS 89-169.

[56] C. W. Uphoff. The art and science of lunar gravity assist. In *Orbital Mechanics and Mission Design*, volume 69 of *Advances in the Astronautical Sciences*, pages 333–346, 1989. AAS 89-170.

[57] J. Wertz, editor. *Spacecraft Attitude Dynamics and Control*. D. Reidel, 1981.

[58] C. G. Zagouras and P. G. Kazantzis. Three-dimensional periodic oscillations generating from plane periodic ones around the collinear Lagrangian points. *Astrophysics and Space Science*, 61:389–409, 1979.